Tectonics®

RESEARCH ARTICLE
10.1029/2023TC007961

# Reconnaissance Basement Geology and Tectonics of North Zealandia

**Nick Mortimer[1], Simon Williams[2], Maria Seton[3], Andy Calvert[4], Tod Waight[5], Rose Turnbull[1], Demian Nelson[6], Mike Palin[7], Jahandar Ramezani[8], Matthew W. Sagar[9], Andy Tulloch[1], Wanda Stratford[9], Julien Collot[10], and Samuel Etienne[10]**

[1]GNS Science Dunedin, Dunedin, New Zealand, [2]University of Tasmania, Hobart, TAS, Australia, [3]University of Sydney, Camperdown, NSW, Australia, [4]US Geological Survey, Menlo Park, CA, USA, [5]Department of Geosciences and Natural Resource Management, University of Copenhagen, Copenhagen, Denmark, [6]University of California, Santa Barbara, Santa Barbara, CA, USA, [7]University of Otago, Dunedin, New Zealand, [8]Massachusetts Institute of Technology, Cambridge, MA, USA, [9]GNS Science, Lower Hutt, New Zealand, [10]Geological Survey of New Caledonia, Noumea, New Caledonia

**Key Points:**

- Basalts and pebbly to cobbly sandstones have been dredged from the Fairway Ridge, Coral Sea
- Dating of the rocks and interpretation of magnetic anomalies allow mapping of major geological units across North Zealandia
- This work completes offshore reconnaissance geological mapping of the entire 5 million square km Zealandia continent

**Supporting Information:**

Supporting Information may be found in the online version of this article.

**Correspondence to:**

N. Mortimer,
n.mortimer@gns.cri.nz

**Citation:**

Mortimer, N., Williams, S., Seton, M., Calvert, A., Waight, T., Turnbull, R., et al. (2023). Reconnaissance basement geology and tectonics of North Zealandia. *Tectonics*, *42*, e2023TC007961. https://doi.org/10.1029/2023TC007961

Received 7 JUN 2023
Accepted 3 SEP 2023

**Author Contributions:**

**Conceptualization:** Nick Mortimer, Simon Williams, Maria Seton
**Formal analysis:** Andy Calvert, Tod Waight, Rose Turnbull, Demian Nelson, Mike Palin, Jahandar Ramezani, Matthew W. Sagar
**Funding acquisition:** Nick Mortimer, Simon Williams, Maria Seton
**Investigation:** Andy Tulloch, Wanda Stratford, Julien Collot, Samuel Etienne
**Methodology:** Nick Mortimer, Simon Williams, Maria Seton
**Writing – original draft:** Nick Mortimer, Simon Williams, Maria Seton
**Writing – review & editing:** Andy Calvert, Tod Waight, Rose Turnbull, Demian Nelson, Mike Palin, Jahandar Ramezani, Matthew W. Sagar, Andy Tulloch, Wanda Stratford, Julien Collot, Samuel Etienne



**Abstract** New rock dredge samples supply key information to establish the tectonic and geological framework of the northern two-thirds of the 95% submerged Zealandia continent. The R/V *Investigator* voyage IN2016T01 to the Fairway Ridge, Coral Sea, obtained poorly sorted poly-lithologic pebbly to cobbly sandstones, well sorted fine grained sandstones, mudstones, bioclastic limestones, and basaltic lavas. Post-cruise analytical work comprised petrography, whole rock geochemical and Sr and Nd isotopic analyses, and U-Pb zircon, Rb-Sr, and Ar-Ar geochronology. A Fairway Ridge cobbly sandstone has a ~95 Ma (early Late Cretaceous) depositional age; two biotite granite cobbles are 111 ± 1 and 128 ± 1 Ma in age, and some volcanic pebbles are also likely Early Cretaceous. Fairway Ridge basalts have intraplate alkaline chemistry and are of Late Eocene age (~40–36 Ma). By analogy with South Zealandia, we interpret strong positive continental magnetic anomalies of North Zealandia to mainly result from Late Cretaceous to Cenozoic intraplate basalts, many of them rift-related lavas. A new basement geological map of North Zealandia shows the position of the Mesozoic Gondwana magmatic arc axis (Median Batholith) and other major geological units. This study completes onland and offshore reconnaissance geological mapping of the entire 5 Mkm$^2$ Zealandia continent.

**Plain Language Summary** To support investigations of the Zealandia continent, we dredged rock samples from the seabed of the Fairway Ridge, Coral Sea. Basalts, sandstones, and pebbles from the sandstones were analyzed and dated. The sandstones are Late Cretaceous (~95 million years old) and contain Early Cretaceous (130–110-million-year-old) granite and volcanic pebbles. The basalts are Eocene (~40 million years old). We have used these results, along with regional magnetic anomaly data, and information from other studies to make a map of the undersea geology of North Zealandia. Onland and offshore reconnaissance geological mapping of the entire 5 Mkm$^2$ Zealandia continent is now complete.

## 1. Introduction

Zealandia is a 95% submerged continent in the SW Pacific Ocean that was formerly part of Gondwana (Mortimer et al., 2017). For most of the Paleozoic and Mesozoic, the south Gondwana margin experienced episodic subduction-related magmatism and terrane accretion. At ~100 Ma long-lived subduction ceased and was replaced by a regime of intracontinental rifting and magmatism that resulted in widespread crustal thinning across Zealandia and West Antarctica. By ~85 Ma (Late Cretaceous) South Zealandia had split from West Antarctica and by ~60 Ma (Paleocene) North Zealandia had split from Australia (e.g., Strogen et al., 2022; Veevers, 2012). During the Paleogene, cooling of the previously thinned Zealandia crust led to its submergence. Today, the Pacific-Australia plate boundary transects the Zealandia continent and divides it into southern and northern parts (Figure 1). Most of the knowledge of the makeup and history of southern Mesozoic Gondwana comes from geological studies of onland New Zealand and New Caledonia (Figure 1). Basement rocks in these countries are typically older than ~105–100 Ma and covering sedimentary basins younger than ~105–100 Ma (e.g., Maurizot et al., 2020a; Mortimer et al., 2014a, 2014b). Basement comprises pre-Late Cretaceous plutonic, metamorphic, and sedimentary rocks divided into deformed batholiths and terranes. Cover comprises Late Cretaceous to Holocene stratified and mainly marine sedimentary rocks in ~30 intracontinental basins. The basins contain subduction-related and/or intraplate volcanic rocks.

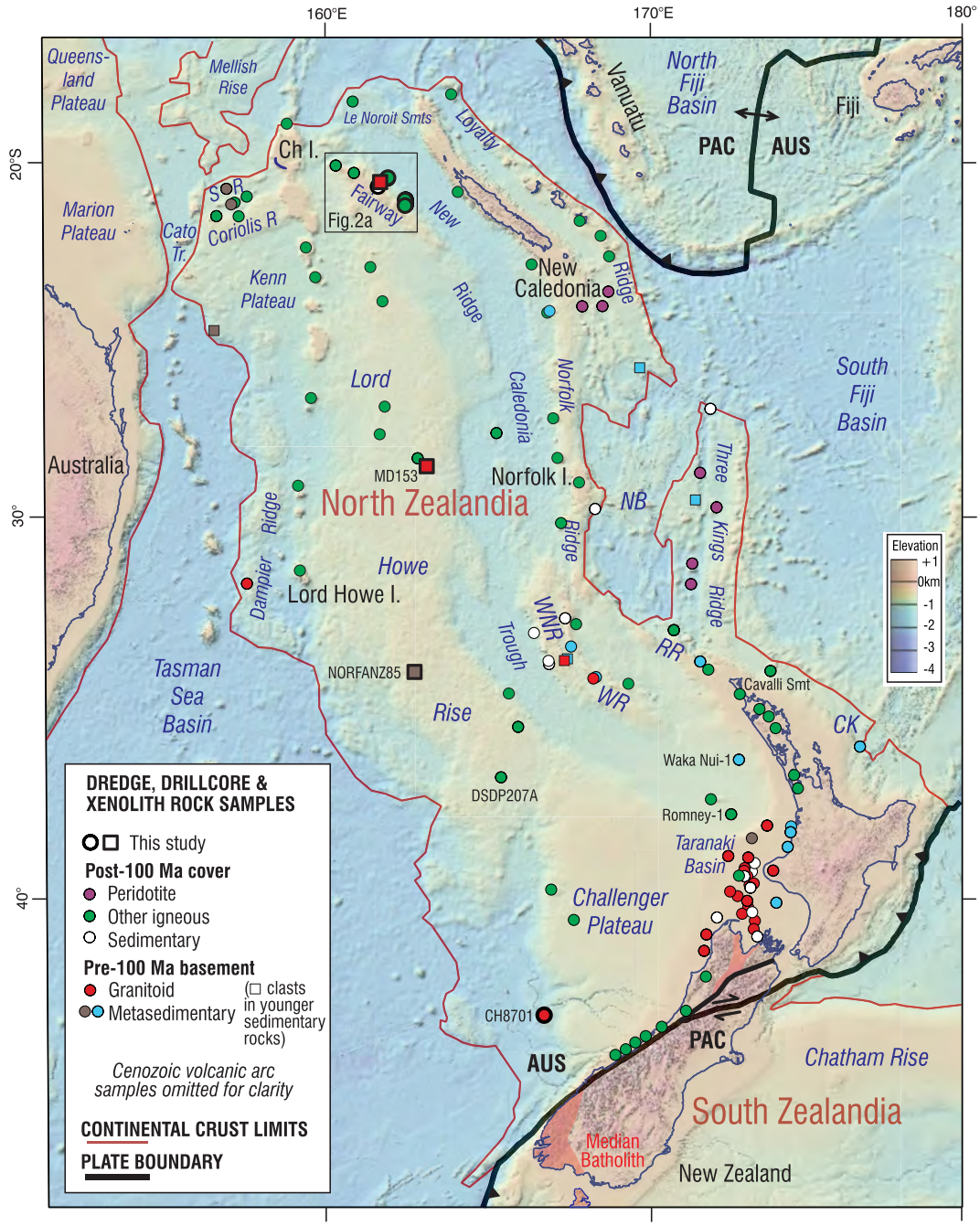


**Figure 1.** Bathymetric and tectonic setting of North Zealandia. Samples analyzed in this paper shown in symbols with thick black outlines. PAC = Pacific Plate, AUS = Australian Plate, Ch I. = Chesterfield Islands, NB = Norfolk Basin, WNR = West Norfolk Ridge, WR = Wanganella Ridge, RR = Reinga Ridge, and CK = Colville Knolls. Data from this study and numerous sources cited in text.

An interpretation of the regional basement geology of 1.5 Mkm$^2$ South Zealandia was presented by Tulloch et al. (2019). They showed a ~1:20M scale geological map with simplified terranes and batholiths, and the pre-breakup continuation of these into West Antarctica. Interpretations were based on analysis of samples from subantarctic islands, oil exploration wells, basement xenoliths, and magnetic anomalies. The purpose of the present paper is to provide a similar interpretation of the basement geology of 3.5 Mkm$^2$ North Zealandia, based on new and existing information. The main data set consists of new geochronological, geochemical, and isotopic analyses of rock samples dredged from the Fairway Ridge (Figures 1 and 2). These supply key information from

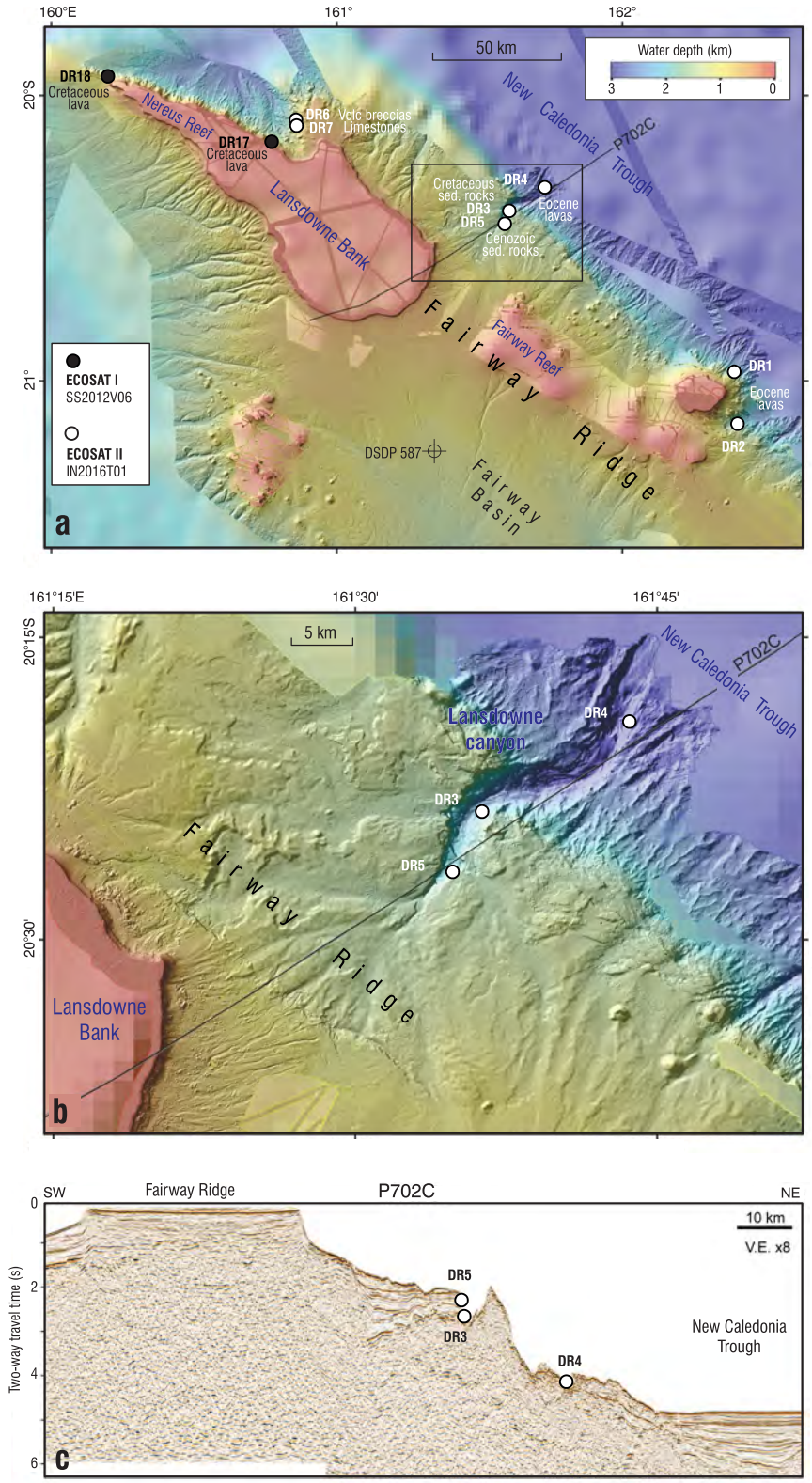


**Figure 2.** Dredge sites on the Fairway Ridge. (a) Regional bathymetric map with SS2012V06 and IN2016T01 dredge sites. (b) Local bathymetric map with IN2016T01 DR3, DR4, and DR5 dredge sites in the incised Lansdowne Canyon. (c) Location of DR3, DR4, and DR5 projected onto previously unpublished Fugro seismic line P702C, vertical exaggeration of water depth is ~8x. Bathymetry data from Smith and Sandwell (1997) and Karthikeyan et al. (2022).

an offshore area near Zealandia's northern margin. We also present new U-Pb ages and Hf and O isotope data for detrital zircons and granite from three previously dredged samples from the Lord Howe Rise and Challenger Plateau (Figure 1, Mortimer et al., 2008, 2015; Tulloch et al., 1991). As well as the rock data, we make qualitative interpretations of regional continental magnetic anomalies of North Zealandia in terms of likely underlying rock units. Collectively, these data and interpretations allow mapping of Paleozoic, Mesozoic, and Cenozoic orogens across North Zealandia along with sedimentary basins and intraplate volcanic rocks. This paper complements Tulloch et al. (2019), and substantially advances the state of knowledge of North Zealandia basement beyond that expressed in Sutherland (1999), Mortimer et al. (2008, 2015, 2018), Collot et al. (2011, 2020), and Higgins et al. (2015).

## 2. Geographic and Geological Setting

North Zealandia includes the major emergent highs of New Zealand and New Caledonia, and major submerged highs of Challenger Plateau, Lord Howe Rise, Norfolk Ridge, and Loyalty Ridge (Figure 1). Smaller ridges such as the Fairway, Coriolis, Dampier, and West Norfolk ridges are separated from the larger positive features and each other by several bathymetric lows of which the New Caledonia Trough is the longest and deepest. Apart from New Zealand and New Caledonia, the only parts of North Zealandia currently above sea level are the Cenozoic volcanic Norfolk, Lord Howe, and Loyalty Islands, and small uninhabited coral sand cays and reefs such as the Chesterfield Islands, and Fairway and Nereus Reefs (Figure 2). The narrow Cato Trough separates Zealandia from the Marion and Queensland Plateaus of the Australian continent. North of Zealandia lies the submerged probable continental crustal fragment of the Mellish Rise (Exon et al., 2006a, 2006b; Gaina et al., 1999).

The Fairway Ridge was first described in the 1970 and 1980 (Mignot, 1984; Ravenne et al., 1977) and its importance as a major geotectonic feature has been reaffirmed in subsequent work for example, Lafoy et al. (2005), Collot et al. (2008, 2017), and Rouillard et al. (2017). The ridge is a ∼400 km-long fault-controlled basement high that separates the New Caledonia and Fairway sedimentary basins. The present-day northern part of the Fairway Ridge is particularly high (shallow) and is interpreted to be the result of an Eocene-Oligocene forebulge-style uplift related to ophiolite emplacement in New Caledonia (Collot et al., 2008). Fairway Reef and Nereus Reef are just exposed at present day sea level (Figure 2). The Lansdowne Bank lies at 100–150 m water depth and would have been emergent at Quaternary low sea level stands. The NE edge of the Fairway Ridge drops steeply into the New Caledonia Trough; the western slopes of the ridge are gentler and the ridge merges with the northern Lord Howe Rise. Using seismic, magnetic and gravity data, the Fairway Ridge can be traced hundreds of km SSE beyond its bathymetric expression and is colinear with the West Norfolk Ridge (Figure 1, Lafoy et al., 2005; Ravenne et al., 1977). The present-day Lansdowne Bank is a partly drowned, isolated carbonate platform (Etienne et al., 2021) that feeds the New Caledonia and Fairway Basins (Pattier et al., 2019). Despite the geophysical literature on the Fairway Ridge, there has been little direct rock sampling. Deep Sea Drilling Project hole 587 intersected Late Miocene, Pliocene and Quaternary calcoozes and skeletal carbonate sands (J. Kennett et al., 1986). Hydrothermally altered Late Cretaceous lavas were dredged from the NW end of the Fairway Ridge by the 2012 ECOSAT I cruise (Figures 1 and 2, Mortimer et al., 2018).

Emergent geological basement in onland New Zealand is divided into two high-level Eastern and Western Provinces. Eastern Province consists of seven Permian to Early Cretaceous metasedimentary-dominated tectonostratigraphic terranes that represent the accretionary wedge and forearc basin parts of a Gondwana margin Mesozoic orogen (Mortimer et al., 2014a, 2014b). Rocks similar to those in the Eastern Province form geological basement in New Caledonia (Maurizot et al., 2020a). The Mesozoic magmatic arc related to the Mesozoic accretionary wedge is the Median Batholith of the Western Province. The rest of the Western Province comprises two Early Paleozoic metasedimentary-dominated terranes intruded by Cambrian to Early Cretaceous plutons (Mortimer et al., 2014a, 2014b). At ∼105–100 Ma, long-lived subduction of Panthalassa oceanic crust under the southern Gondwana margin ceased and was replaced by a continental rift regime that ultimately led (from ∼85 Ma) to breakaway of a thinned Zealandia continent from Gondwana that became progressively submerged. This rift and drift geological record consists of sedimentary basins and intraplate volcanic rocks. From the Eocene, the northeastern part of Zealandia was overprinted by ophiolitic allochthons and subduction-related volcanic rocks that is, components of a Cenozoic orogen (Maurizot et al., 2020b; Mortimer et al., 2014a, 2014b).

Dredge sampling in the last 25 years has allowed extrapolation of the Median Batholith (one of the major basement units) north from New Zealand to ∼34°S (Mortimer et al., 1998) and then to ∼28°S (Mortimer et al., 2015).

**Table 1**
*Location and Rock Type Summary*

| Cruise | Dredge | Longitude (°E) | Latitude (°S) | Depth (m) | Quantity (kg) | Location | Sample description | GNS P# | References |
|---|---|---|---|---|---|---|---|---|---|
| IN2016T1 | 1 | 162.401 | 20.961 | 2000 | 3 | Fairway Ridge | Mostly limestone, some volcanic breccia | 85718 | Williams et al. (2016), Mortimer et al. (2019), and This study |
| IN2016T1 | 2 | 162.403 | 21.153 | 1,600 | 200 | Fairway Ridge | Mostly limestone, some volcanic breccia | 85719–21 | Williams et al. (2016), Mortimer et al. (2019), and This study |
| IN2016T1 | 3 | 161.604 | 20.396 | 2150 | 400 | Fairway Ridge | Mostly limestone, lesser sst & pebbly cobbly sst | 85722–30 | Williams et al. (2016) and This study |
| IN2016T1 | 4 | 161.727 | 20.320 | 3,100 | 200 | Fairway Ridge | Mostly limestone, some basalt, mudstone | 85731–34 | Williams et al. (2016) and This study |
| IN2016T1 | 5 | 161.581 | 20.441 | 1,900 | 30 | Fairway Ridge | Mostly varitextured limestones, some mudstone | 85735 | Williams et al. (2016) |
| IN2016T1 | 6 | 160.857 | 20.077 | 1,500 | 35 | Fairway Ridge | Mostly limestone, some altered volcanic breccia | 85736 | Williams et al. (2016) |
| IN2016T1 | 7 | 160.857 | 20.094 | 1,350 | 40 | Fairway Ridge | Soft white limestone | na | Williams et al. (2016) |
| MD153 | 1 | 163.063 | 28.630 | 1,650 | na | N Lord Howe Rise | Granitic pebbly sandstone, manganese crusts | 81390 | This study and Mortimer et al. (2015) |
| TAN0308 | Tow85 | 162.677 | 34.232 | 515 | na | S Lord Howe Rise | Volcanic breccia with rare greywacke and schist clasts | 69782 | This study and Mortimer et al. (2008) |
| CH8701 | 1 | 166.80 | 42.77 | 3,000 | na | Challenger Plateau | Weathered biotite granite | 44932 | Tulloch et al. (1991) |

*Note.* Samples analyzed in this paper are underlined.

However, its position and strike north of 28°S have, until now, remained speculative. Other major unknowns have been the areal extent of Late Cretaceous to Pliocene igneous rocks in North Zealandia and their cause (which of them relate to intraplate rifting and which to subduction).

## 3. Rock Samples

### 3.1. IN2016T01 Voyage

ECOSAT II (Eastern COral SeA Tectonics II) was the geological component of the July 2016 IN2016T01 Lautoka to Hobart transit voyage by the Australian ship R/V *Investigator* (Williams et al., 2016). ECOSAT II was a follow-up to the 2012 ECOSAT I voyage (Mortimer et al., 2018; Seton et al., 2016). Table 1 summarizes the seven rock dredge (DR) deployments of ECOSAT II that were made in three steep rocky areas along the NE-facing scarp of the Fairway Ridge (Figure 2). An estimated 900 kg of igneous and sedimentary rock was dredged of which 102 kg was retained for study and archiving (Williams et al., 2016).

IN2016T01 DR1–2 and DR5–7 are not the main topic of this paper but are mentioned here for completeness. DR1 and DR2 were made on and near a 15 km diameter guyot-like feature (Figure 2a). Post-cruise work confirmed the guyot as an alkaline to nephelinitic intraplate volcano dated as Eocene by foraminifera in limestones (Mortimer et al., 2019). DR5 was made in the upper part of a submarine canyon incised into the NE side of Lansdowne Bank (Figure 2b); about 30 kg of rock was recovered comprising ~95% varitextured limestones and ~5% olive gray mudstone with minor sponge and coral fragments. DR6 and DR7 were made on the Fairway Ridge scarp, ~150 km NW of the aforementioned guyot. Alkaline hyaloclastite breccia was obtained at DR6 and limestones at DR7.

IN2016T01 DR3 and DR4 are the main topic of this paper. Like DR5, these were made in a submarine canyon incised into the northeast side of Lansdowne Bank (Figure 2b). We refer to this feature as Lansdowne canyon (informal name). A seismic line near the canyon (Figure 2c) provide stratigraphic context for the dredges. DR3 was made in the middle part of the canyon. About 400 kg of rock was recovered, comprising ~60% varitextured bioclastic and micritic limestones, ~20% cobbly and pebbly coarse sandstones, and ~20% non-pebbly medium- to fine-grained sandstones and carbonaceous mudstones; unconsolidated white clay was a minor rock type. DR4 was made in the lower part of Lansdowne canyon; about 200 kg of rock was recovered comprising ~90% varitextured bioclastic and micritic limestones and ~10% fractured basaltic and hypabyssal rocks; carbonaceous muddy sandstone was a minor rock type. The abundance of bioclastic limestone in all three Lansdowne canyon dredges indicates that much Neogene reef debris has slumped down the face of the Fairway ridge scarp.

### 3.2. Fairway Ridge DR3 and DR4 Samples

In Lansdowne canyon, our dredging at site DR3 was intended to target seismic acoustic basement, although the dredge appears to have recovered rocks from the lowermost sedimentary cover (Figures 2c and 3a). Our newly studied samples from IN2016T01 DR3 are as follows: P85724 (DR3Aiii of Williams et al. (2016)) is a single ~30 × 30 × 30 cm block of hard, pale olive, poorly sorted, coarse- to very coarse-grained pebbly to cobbly sandstone (Figure 3a). Bedding, grading and other structures are not visible; the cobbles and pebbles are plutonic and volcanic. Based on visual estimates of the sandstone in thin section, the P85724 sandstone matrix has ~5% porosity and a quartz: feldspar:

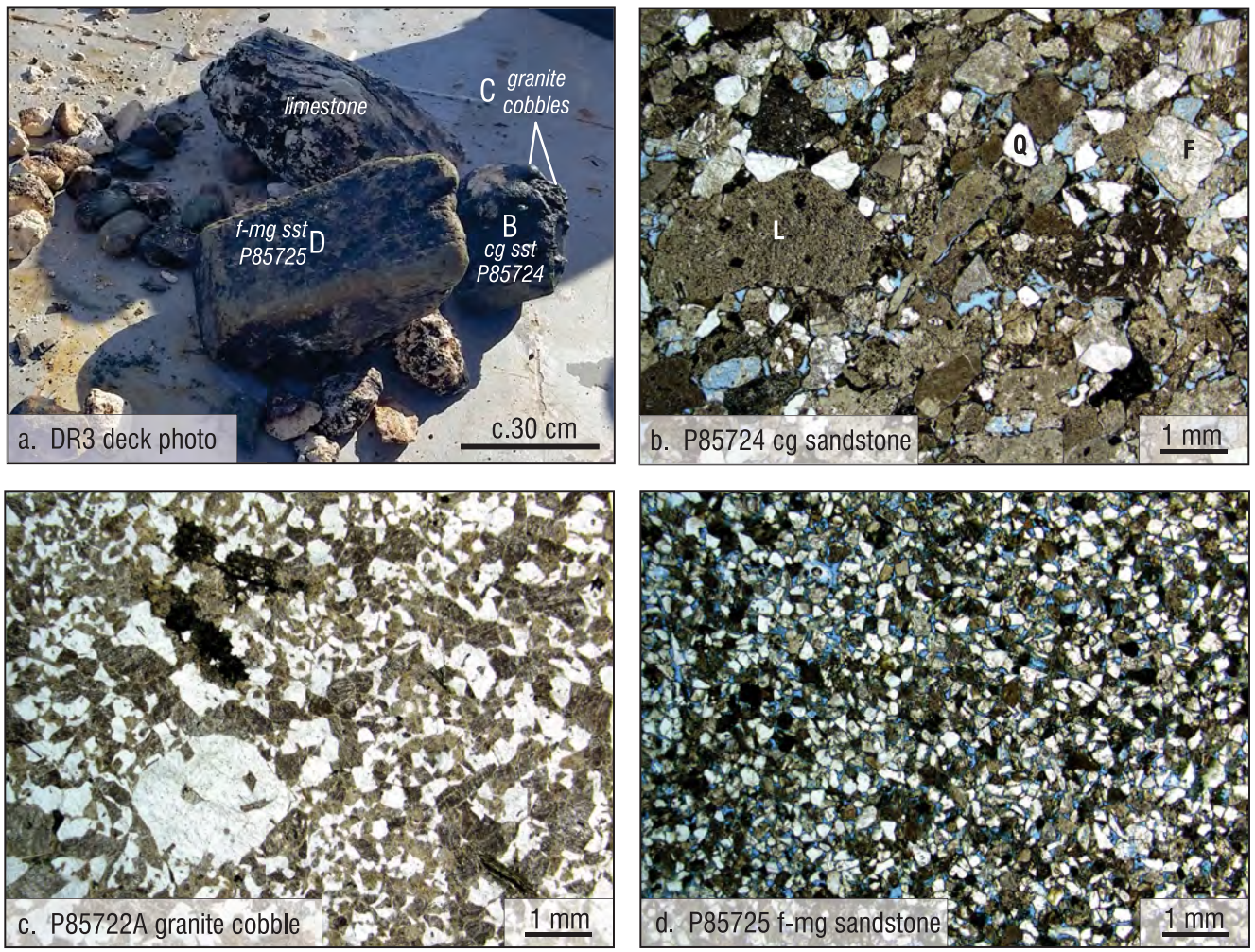


**Figure 3.** (a) IN2016T01 DR3 deck image showing blocks of limestone (pale), sandstone, pebbly to cobbly sandstone, and disaggregated cobbles. The large sandstone slab is ~0.5 m long. (b) Photomicrograph of coarse-grained lithic cobbly sandstone matrix P85724 (Q = quartz, F = feldspar, and L = lithic grain). (c) Photomicrograph of granophyric biotite granite cobble P85722A. (d) Photomicrograph of fine-medium grained sandstone P85725. All photomicrographs taken in plane polarized light. Porosity indicated by blue-stained epoxy.

lithic (QFL) ratio of detrital grains ~10:25:65. The volcanic: sedimentary: metamorphic lithics ratio ($L_v$:$L_s$:$L_m$) is ~85:14:1, with most of the volcanic grains being siliceous (Figure 3b). Detrital biotite is common, and detrital epidote, chlorite, zircon, and organic carbon fragments occur in lesser to trace amounts. Some authigenic pumpellyite was noted in the sandstone matrix. Six individual cobbles from the P85724 (DR3Aiii) pebbly to cobbly sandstone were selected for further study: P85722A, B and C are phaneritic biotite granites (Figure 3c), P85723A is a dacite, P85723B a brecciated andesite, and P85723C a rhyolite.

P85725 (DR3B) is a single ~50 × 50 × 30 cm slab of hard, moderate olive brown, well-sorted, fine-grained sandstone (Figure 3a). In thin section this has 5%–10% porosity, QFL ~30:50:20 and $L_v$:$L_s$:$L_m$ ~90:1:9 (Figure 3d). Detrital biotite is common and detrital zircon, tourmaline, garnet, pale amphibole, and carbonaceous material were noted. P85725 had some mudstone partings, plant fragments and burrows; it also exhibits a sharp planar change in color to a greyish olive half, likely a chemical reaction front.

Our dredging in the deeper part of Lansdowne canyon at IN2016T01 DR4 sampled the flank of the canyon (Figure 2c). Four rock types were identified and analyzed. P85731 (DR4Ai) is one of several cobble- to pebble-sized pieces of hard, medium dark gray to olive gray, very fine-grained microlitic aphyric basalt with calcite amygdules. P85732 (DR4Aii) is one of several cobble- to pebble-sized pieces of hard, medium dark gray fresh to moderately altered aphanitic lava with abundant 2–3 mm calcite amygdules and some phosphatic

infillings. P85733 (DR4B) is from a single separate 50 × 20 × 20 cm boulder of pervasively fractured but hard, medium dark gray, medium-grained non-amygdaloidal dolerite. P85734 (DR4C) is one of three dm-sized pieces of moderately hard, olive gray, relatively well-sorted, very fine-grained muddy non-calcareous carbonaceous sandstone which lacks lamination and other bedding structures.

### 3.3. Lord Howe Rise and Challenger Plateau Samples

While work on IN2016T01 DR3 and 4 Fairway Ridge samples underpins most of this paper, we also report results of new U-Pb dating and Lu-Hf and O isotopic analysis of zircons from three previously studied Lord Howe Rise and Challenger Plateau samples (Figure 1). One is P81390, a poorly sorted plutoniclastic pebbly sandstone from an MD153 dredge on the central Lord Howe Rise at latitude 28.6°S (Mortimer et al., 2015). Another is P69782, a moderately sorted polymict volcanic very fine pebble breccia from a NORFANZ85 dredge on the southern Lord Howe Rise near latitude 34.2°S (Mortimer et al., 2008). The third is P44932, an altered biotite granite from a CH8701 dredge on a horst on the Challenger Plateau near latitude 42.8°S (Tulloch et al., 1991).

## 4. Analytical Methods

Rocks and minerals were processed and analyzed at several laboratories (Supplemental File 1 in Supporting Information S2). Thin section preparation, rock crushing and mineral separation were done at GNS Science, Lower Hutt, and Dunedin. After removing visibly altered rind and fracture fill material, slices of rock were soaked in deionized water for 3 days to leach seawater. After drying, rocks were crushed to fine powders in a tungsten carbide ring mill. Mineral separates for dating were made by successive crushing, sieving, density separation in sodium polytungstate and methylene iodide heavy liquids, magnetic separation, and handpicking. Zircons with diverse size, shape, and color, and with relatively few inclusions, were picked. Cathodoluminescence (rather than backscattered electron) images were taken of polished and epoxy-mounted zircons prior to their analysis at the University of Otago and University of California Santa Barbara (UCSB) (Supplemental File 2 in Supporting Information S2).

Major and trace elements were analyzed on fused beads at ALS Laboratories, Brisbane (https://www.alsglobal.com). Majors were analyzed by inductively coupled plasma-atomic emission spectrometry using ALS's ME-ICP06 package, and traces were analyzed by ICP-MS (mass spectrometry) using ALS's ME-MS81 package. Separate aliquots of powder were analyzed for Rb, Sr, Sm and Nd, and for Sr and Nd isotopes by isotope dilution thermal ionization mass spectrometry (ID-TIMS) method at the University of Copenhagen, following methods described in van der Meer et al. (2018) and Borst et al. (2018).

U-Pb geochronology and trace element analysis of zircons at the University of Otago, Dunedin, New Zealand used laser ablation (LA-) ICP-MS methods mostly following the procedures described in Mortimer et al. (2015). U-Pb, trace element and Hf isotope analyses of zircons at the UCSB used laser ablation ICP-MS methods following procedures described in Nelson and Cottle (2017). Zircon U-Pb geochronology by CA- (chemical abrasion) ID-TIMS was done at the Massachusetts Institute of Technology Isotope Laboratory following procedures described in Ramezani et al. (2022). Zircon O-isotope analysis at the Universität Heidelberg and zircon Lu-Hf isotope analysis at Curtin University were undertaken by secondary ion mass spectrometry and multi-collector LA-ICP-MS respectively, according to procedures documented in Turnbull et al. (2021). All U-Pb age calculations and statistical assessment of detrital zircon populations were completed using Isoplot software (Ludwig, 2008). For ages established in this study using ICP-MS methods, only $^{238}U/^{206}Pb$ ages that were <10% discordant were used for age calculations (for grains <1,500 Ma, concordance = $^{206}Pb$-$^{238}U/^{207}Pb$-$^{235}U$. For grains >1,500 Ma, concordance = $^{206}Pb$-$^{238}U/^{207}Pb$-$^{206}Pb$).

Ar-Ar dating was done at the United States Geological Survey, Menlo Park following procedures in Calvert and Lanphere (2006); Ar-Ar ages in this paper are reported relative to a Fish Canyon sanidine age of 28.198 Ma (i.e., they are compatible with Gans et al. (2023)).

There is good coverage of regional-scale magnetic potential field data across and near North Zealandia (e.g., Collot et al., 2009; Lafoy et al., 2005; Lapouille, 1977; Meyer et al., 2017; Schreckenberger et al., 1992; Sutherland, 1999). In this paper we have masked flanking oceanic crust anomalies and used the Meyer et al. (2017) EMAG2 compilation to make interpretations of continental magnetic anomalies within Zealandia.

More detailed descriptions of analytical methods are given in Supplemental File 1 in Supporting Information S2 and analytical data are given in Supplemental Files 2–8 in Supporting Information S2 (Mortimer et al., 2023). Additionally, the United States Geological Survey geochronology data are reported in a separate data release (Calvert, 2023). All samples, powders and mineral separates are lodged in the GNS Science Petrology Collection (to which the prefix "P" refers). Associated data are stored in the Petlab database (http://pet.gns.cri.nz, Strong et al., 2016).

## 5. Results

### 5.1. Whole Rock Geochemistry

New whole rock geochemical and isotopic data for IN2016T01 DR3 and 4 samples are given in Table 2 and plotted in Figure 4. In all cases, we use the data to define and interpret compositions in a general rather than a precise way. This is because of the small sample set, and the mineralogically altered nature of many samples. While primary textures of igneous rocks are well preserved, feldspars are inevitably turbid and glassy matrix of volcanic rocks is devitrified. Amygdaloidal lava P85732 has anomalously high (1.26 wt %) $P_2O_5$ because of secondary phosphate infiltration. With these caveats, on a silica-total alkalis diagram (Figure 4a) four distinct geochemical groups are obvious, corresponding to the four different rock type groups: DR1, 2 and 4 basaltic lavas, DR3 granite cobbles, DR3 volcanic pebbles and DR3 and 4 clastic sedimentary rocks.

The basaltic rocks from IN2016T1 DR1, DR2 and DR4 all have low silica. The DR4 samples are alkali basalts to trachybasalts but, as shown by their higher $SiO_2$ and lower Nb/Y (Figures 4a and 4b), they are different from the nephelinitic to basanitic compositions of the DR1 and DR2 lavas reported by Mortimer et al. (2019). On multi-element MORB-normalized and Nb/Yb versus Th/Yb diagrams (Figures 4c and 4d) the DR4 lavas are enriched in incompatible elements and have signatures similar to intraplate basaltic lavas. The least altered DR4 sample, P85733, was analyzed for Sr and Nd isotopes and, as shown in Figure 4f, it lies within the range of many "low $SiO_2$" (i.e., alkaline) intraplate Zealandia basalts.

The three analyzed DR3 biotite granite cobbles are all very fractionated. This is evident in their extreme (>75 wt %) $SiO_2$, Zr/Ti (Figures 4a and 4b), troughs at Ba, P and Ti on the Normal mid-ocean ridge basalt normalized multi-element diagram (Figure 4c) and other extreme element ratios such as Rb/Sr. Their highly fractionated nature makes it difficult to use standard granitoid geochemical parameters to characterize their I, S or A-type nature (Tulloch et al., 2019). However, in Figure 4e their Nb + Y and Rb contents are low to moderate enough to plot in the magmatic arc field instead of collisional or within-plate fields. Nb/Yb ratios <10 also indicate that the granites have affinities with continental arc rather than alkaline intraplate igneous rock series (Figure 4d). Isotopically, they lie within or close to the fields of New Zealand Mesozoic I-type plutonic Darran and Separation Point suites and lack the distinctive radiogenic Sr and non-radiogenic Nd of S-type granitoids (Figure 4f).

The three DR3 volcanic cobbles are intermediate to siliceous igneous rocks (a high-silica andesite, a dacite and a rhyolite). Precise rock nomenclature is ambiguous, likely because of element mobility; however, they are not as fractionated as the granites (Figures 4a–4d). In all key aspects of bulk chemical and isotopic composition (e.g., Nb/Y, Th/Yb) they are seemingly of typical (unexceptional) subalkaline composition. On the MORB-normalized multi-element plot they also show enrichment in large-ion lithophile elements Cs, Rb, Ba, and Th and a depletion in high field strength elements Nb, Ta, and Ti. This is typical of lavas in subduction-related settings.

Three Fairway Ridge sandstones from DR3 and DR4 are also plotted in some parts of Figure 4. Roser and Korsch (1986) have shown that igneous rock plots can be useful to establish the broad geochemical nature of sandstone source areas, especially for lithic-rich sandstones. As expected, the Fairway Ridge quartzofeldspathic sandstone has the highest $SiO_2$, and the muddy sandstone the lowest (Figure 4a).

The Challenger Plateau granite P44932 from dredge CH8701 was too altered and penetrated by manganese crust for whole rock geochemistry, but apatite separated from the granite gave an $^{87}Sr/^{86}Sr$ ratio of 0.71845 (Tulloch et al., 1991). In New Zealand, such high initial ratios are distinctive of the Devonian S-type Paleozoic Karamea Suite (Figure 4f).

### 5.2. U-Pb Zircon Geochronology

#### 5.2.1. Fairway Ridge

Interpretation of U-Pb zircon ages from the two Fairway Ridge granite cobbles is straightforward. Zircon grains in P85722A are all euhedral and there is a well-defined 111.3 ± 1.1 $^{206}Pb^*/^{238}U$ Ma age (where * indicates

Tectonics

10.1029/2023TC007961

**Table 2**
*Whole Rock Geochemical and Isotopic Data*

| | Igneous rocks | | | | | | | | | Sedimentary rocks | | |
|---|---|---|---|---|---|---|---|---|---|---|---|---|
| GNS P# | 85722A | 85722C | 85722B | 85723B | 85723A | 85723C | 85731 | 85732 | 85733 | 85724 | 85725 | 85734 |
| Dredge | DR3Ai | DR3Ai | DR3Ai | DR3Aii | DR3Aii | DR3Aii | DR4Ai | DR4Aii | DR4B | DR3Aiii | DR3B | DR4C |
| Rock | Bi granite clast | Bi granite clast | Bi granite clast | Andesite clast | Dacite clast | Rhyolite clast | Vfg basalt | Aphyric basalt | Fractured dolerite | Cg pebbly sst matrix | Well-srtd, f-mg sst | Vfg muddy sst |
| $SiO_2$ (wt%) | 77.70 | 77.00 | 79.20 | 62.30 | 65.10 | 68.20 | 47.10 | 48.40 | 48.30 | 68.90 | 73.90 | 63.00 |
| $TiO_2$ | 0.12 | 0.13 | 0.11 | 1.23 | 0.71 | 0.82 | 2.06 | 2.26 | 1.83 | 0.59 | 0.60 | 0.98 |
| $Al_2O_3$ | 11.90 | 12.70 | 12.15 | 15.35 | 16.75 | 13.85 | 15.45 | 15.95 | 13.80 | 14.15 | 13.60 | 16.60 |
| $Fe_2O_3T$ | 1.30 | 1.33 | 1.06 | 6.73 | 3.56 | 5.66 | 10.55 | 13.00 | 12.50 | 4.05 | 3.64 | 8.14 |
| MnO | 0.01 | 0.02 | 0.01 | 0.12 | 0.05 | 0.08 | 0.12 | 0.09 | 0.13 | 0.06 | 0.05 | 0.03 |
| MgO | 0.24 | 0.25 | 0.21 | 2.18 | 1.64 | 1.87 | 4.15 | 3.04 | 8.83 | 1.84 | 1.25 | 1.79 |
| CaO | 0.15 | 1.05 | 0.54 | 2.51 | 0.57 | 0.56 | 10.45 | 9.26 | 5.93 | 0.72 | 1.53 | 1.07 |
| $Na_2O$ | 3.28 | 2.88 | 3.21 | 5.34 | 7.75 | 5.03 | 4.06 | 3.85 | 4.00 | 4.19 | 3.04 | 3.03 |
| $K_2O$ | 4.54 | 5.36 | 4.98 | 1.60 | 1.42 | 2.11 | 0.88 | 1.45 | 1.11 | 2.34 | 2.58 | 2.27 |
| $P_2O_5$ | 0.01 | 0.04 | 0.02 | 0.38 | 0.22 | 0.21 | 0.42 | 1.26 | 0.33 | 0.12 | 0.08 | 0.11 |
| LOI | 0.61 | 0.40 | 0.30 | 2.23 | 1.48 | 1.64 | 3.55 | 1.54 | 3.11 | 2.06 | 1.52 | 3.68 |
| Total | 99.86 | 101.16 | 101.79 | 99.97 | 99.25 | 100.03 | 98.79 | 100.10 | 99.87 | 99.02 | 101.79 | 100.70 |
| V (ppm) | 6 | 22 | 16 | 116 | 89 | 85 | 171 | 239 | 162 | 77 | 79 | 214 |
| Cr | 10 | 10 | <10 | 20 | 20 | 10 | 160 | 320 | 330 | 20 | 30 | 40 |
| Ga | 14.3 | 13.2 | 13.0 | 22.1 | 14.7 | 15.5 | 24.9 | 26.8 | 21.5 | 18.8 | 16.4 | 18.9 |
| Rb | 141.0 | 189.0 | 205.0 | 43.3 | 31.9 | 74.5 | 15.6 | 28.5 | 20.5 | 57.9 | 70.4 | 74.0 |
| Sr | 51.5 | 163.5 | 65.8 | 326.0 | 203.0 | 147.0 | 653.0 | 633.0 | 339.0 | 119.5 | 286.0 | 123.5 |
| Y | 12.0 | 8.6 | 14.5 | 43.1 | 9.8 | 24.1 | 22.0 | 33.4 | 20.0 | 21.4 | 15.4 | 22.1 |
| Zr | 99 | 99 | 97 | 258 | 134 | 284 | 195 | 199 | 155 | 190 | 205 | 161 |
| Nb | 6.9 | 10.5 | 11.1 | 11.2 | 4.1 | 7.7 | 45.2 | 47.9 | 33.8 | 6.8 | 6.3 | 6.3 |
| Cs | 1.36 | 1.74 | 1.59 | 0.79 | 0.25 | 1.29 | 0.09 | 0.52 | 0.22 | 1.48 | 4.02 | 2.52 |
| Ba | 409 | 411 | 209 | 380 | 423 | 317 | 272 | 269 | 319 | 324 | 446 | 279 |
| La | 26.8 | 17.6 | 30.5 | 39.1 | 8.8 | 17.4 | 30.1 | 38.1 | 22.2 | 21.9 | 20.0 | 15.0 |
| Ce | 50.4 | 31.9 | 58.4 | 86.1 | 23.6 | 39.8 | 59.3 | 67.2 | 44.3 | 45.3 | 41.2 | 33.3 |
| Pr | 5.28 | 3.26 | 5.93 | 11.2 | 3.45 | 5.26 | 7.30 | 8.48 | 5.42 | 5.53 | 4.98 | 4.07 |
| Nd | 18.1 | 10.6 | 19.4 | 46.0 | 15.0 | 21.7 | 29.9 | 34.6 | 22.7 | 21.9 | 19.1 | 17.1 |
| Sm | 3.11 | 1.69 | 3.14 | 9.50 | 2.76 | 4.81 | 6.39 | 7.36 | 4.91 | 4.27 | 3.59 | 3.83 |
| Eu | 0.30 | 0.64 | 0.45 | 2.81 | 0.60 | 0.94 | 2.39 | 2.73 | 1.87 | 1.05 | 1.08 | 1.08 |
| Gd | 2.55 | 1.54 | 2.63 | 9.63 | 2.64 | 4.98 | 6.48 | 7.87 | 5.50 | 4.23 | 3.23 | 4.09 |
| Tb | 0.35 | 0.22 | 0.38 | 1.35 | 0.35 | 0.72 | 0.89 | 1.12 | 0.75 | 0.62 | 0.45 | 0.66 |

Tectonics
10.1029/2023TC007961

**Table 2**
*Continued*

| | Igneous rocks | | | | | | | | | Sedimentary rocks | | |
|---|---|---|---|---|---|---|---|---|---|---|---|---|
| GNS P# | 85722A | 85722C | 85722B | 85723B | 85723A | 85723C | 85731 | 85732 | 85733 | 85724 | 85725 | 85734 |
| Dredge | DR3Ai | DR3Ai | DR3Ai | DR3Aii | DR3Aii | DR3Aii | DR4Ai | DR4Aii | DR4B | DR3Aiii | DR3B | DR4C |
| Rock | Bi granite clast | Bi granite clast | Bi granite clast | Andesite clast | Dacite clast | Rhyolite clast | Vfg basalt | Aphyric basalt | Fractured dolerite | Cg pebbly sst matrix | Well-srtd, f-mg sst | Vfg muddy sst |
| Dy | 2.09 | 1.38 | 2.30 | 7.94 | 1.94 | 4.47 | 4.86 | 6.33 | 4.29 | 3.74 | 2.79 | 4.34 |
| Ho | 0.40 | 0.29 | 0.47 | 1.56 | 0.35 | 0.89 | 0.83 | 1.11 | 0.76 | 0.76 | 0.56 | 0.90 |
| Er | 1.14 | 0.95 | 1.48 | 4.64 | 0.99 | 2.72 | 2.12 | 3.00 | 1.90 | 2.36 | 1.70 | 2.60 |
| Tm | 0.20 | 0.16 | 0.25 | 0.67 | 0.14 | 0.41 | 0.27 | 0.39 | 0.24 | 0.36 | 0.25 | 0.42 |
| Yb | 1.41 | 1.20 | 1.87 | 4.51 | 0.90 | 2.80 | 1.69 | 2.45 | 1.51 | 2.48 | 1.75 | 2.73 |
| Lu | 0.22 | 0.21 | 0.32 | 0.68 | 0.13 | 0.45 | 0.23 | 0.37 | 0.22 | 0.38 | 0.27 | 0.41 |
| Hf | 2.8 | 3.3 | 3.5 | 6.8 | 3.6 | 7.2 | 5.0 | 5.0 | 3.8 | 5.2 | 5.4 | 4.8 |
| Ta | 0.9 | 1.6 | 1.7 | 0.8 | 0.3 | 0.7 | 2.8 | 2.9 | 2.1 | 0.6 | 0.5 | 0.5 |
| Th | 18.10 | 26.50 | 33.90 | 5.11 | 2.90 | 8.71 | 4.01 | 4.11 | 2.96 | 9.25 | 7.28 | 6.20 |
| U | 1.43 | 2.43 | 2.86 | 1.35 | 1.83 | 1.99 | 1.05 | 1.61 | 0.82 | 2.00 | 1.33 | 1.38 |
| Rb | 129.07 | 169.72 | – | 37.89 | 27.16 | 65.32 | – | – | 18.02 | – | – | – |
| Sr | 50.47 | 161.17 | – | 326.23 | 198.63 | 145.73 | – | – | 333.89 | – | – | – |
| Nd | 27.72 | 43.00 | – | 48.42 | 37.80 | 37.18 | – | – | 53.02 | – | – | – |
| Sm | 4.64 | 7.21 | – | 10.26 | 7.76 | 8.35 | – | – | 12.17 | – | – | – |
| $^{87}Rb/^{86}Sr$ | 7.405 | 3.047 | – | 0.336 | 0.395 | 1.296 | – | – | 0.156 | – | – | – |
| $^{87}Sr/^{86}Sr$ | 0.716012 | 0.709521 | – | 0.704116 | 0.704204 | 0.705798 | – | – | 0.703699 | – | – | – |
| $^{87}Sr/^{86}Sr$ 2σ error | 0.000004 | 0.000004 | – | 0.000004 | 0.000004 | 0.000004 | – | – | 0.000004 | – | – | – |
| $^{147}Sm/^{144}Nd$ | 0.1011 | 0.1012 | – | 0.1279 | 0.1239 | 0.1355 | – | – | 0.1386 | – | – | – |
| $^{143}Nd/^{144}Nd$ | 0.512674 | 0.512670 | – | 0.512759 | 0.512730 | 0.512706 | – | – | 0.512923 | – | – | – |
| $^{143}Nd/^{144}Nd$ 2σ error | 0.000007 | 0.000006 | – | 0.000006 | 0.000006 | 0.000006 | – | – | 0.000005 | – | – | – |
| Age (Ma) | 111 | 128 | – | 127 | 127 | 127 | – | – | 36 | – | – | – |
| $^{87}Sr/^{86}Sr$ initial | 0.704437 | 0.703978 | – | 0.703510 | 0.703490 | 0.703458 | – | – | 0.703619 | – | – | – |
| $^{143}Nd/^{144}Nd$ initial | 0.512601 | 0.512585 | – | 0.512652 | 0.512627 | 0.512594 | – | – | 0.512891 | – | – | – |
| εNd initial | 2.1 | 2.2 | – | 3.5 | 3.0 | 2.3 | – | – | 5.8 | – | – | – |

*Note*. For whole rock compositions of IN2016T1 DR1 and DR2 lavas see Mortimer et al. (2019).

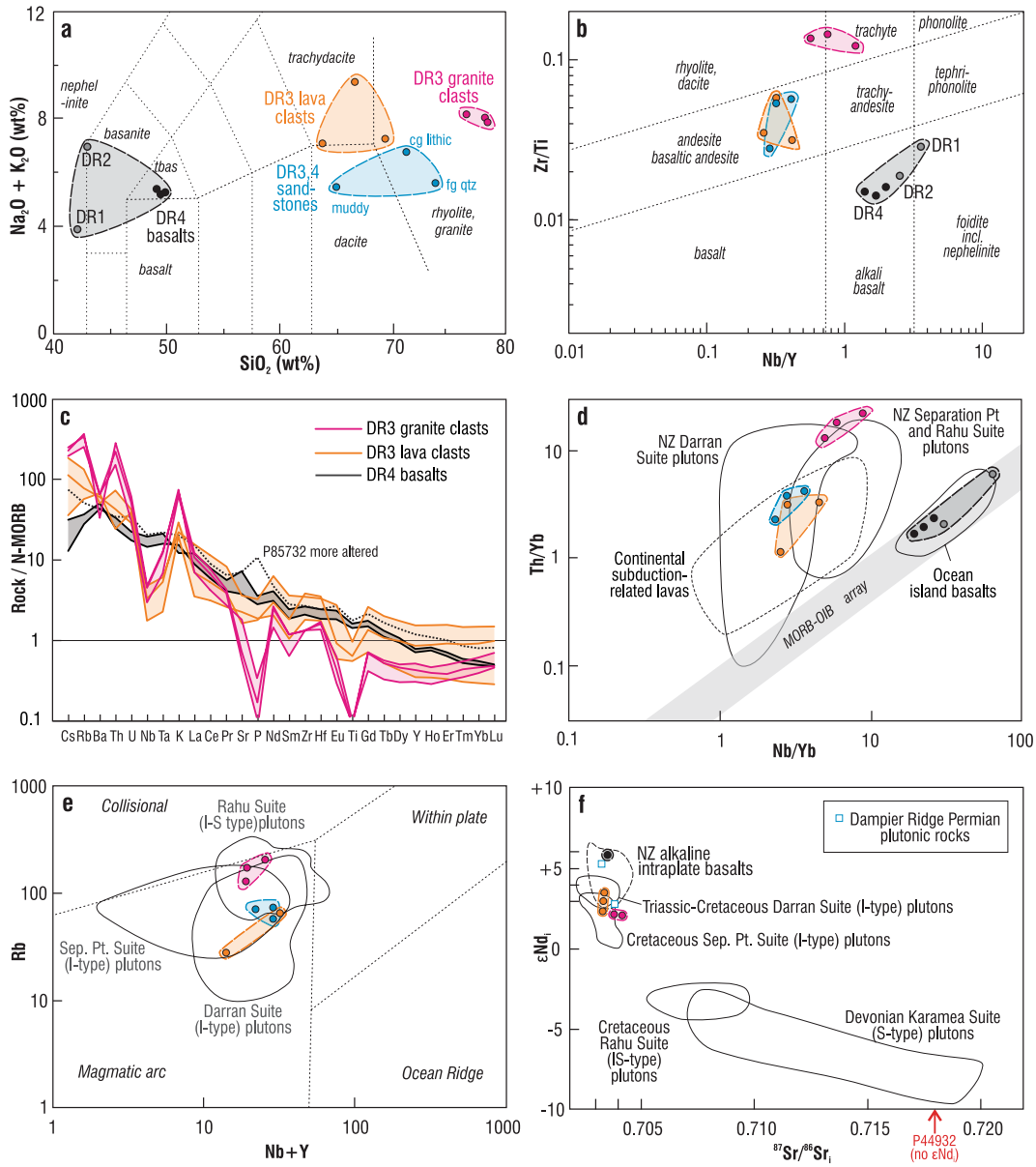


**Figure 4.** Binary whole rock geochemical diagrams of IN2016T01 Fairway Ridge samples. (a) $SiO_2$ versus total alkalis (Le Maitre, 1989). (b) Nb/Y versus Zr/Ti (Pearce, 1996). (c) Normal mid-ocean ridge basalt normalized multi-element plot (Sun & McDonough, 1989). (d) Nb/Yb versus Th/Yb (Pearce, 1996), reference fields are compiled from Muir et al. (1995, 1998), Price et al. (2011), and Sagar et al. (2016). (e) Nb + Y versus Rb (Förster et al., 1997; Pearce et al., 1984), note only siliceous igneous and sedimentary rocks are plotted. (f) $^{87}Sr/^{86}Sr$ versus εNd initial isotope ratios. P44932 from Tulloch et al. (1991), Dampier Ridge from McDougall et al. (1994), reference fields from Timm et al. (2010), Turnbull et al. (2016), and Tulloch et al. (2019). Symbol colors in panel (a) apply to all panels.

age corrected for common Pb) based on 10 concordant analyses (Figure 5a). Three spots were distinctly older than this; the 131 Ma age is from a separate euhedral grain, and the two Cambrian ages are core and rim spots on a euhedral grain (Supplemental Files 2 and 3 in Supporting Information S2). Zircon grains in P85722C are euhedral and anhedral and a well-defined 128.2 ± 1.2 Ma $^{206}Pb^*/^{238}U$ age is based on 12 concordant analyses (Figure 5b). P85722C contained no substantially older zircons and also has slightly lower radiogenic Sr and higher radiogenic Nd compared with P85722A (Table 2).

Almost all zircon grains in the Fairway Ridge coarse volcanic-lithic sandstone matrix of cobbly sandstone P85724 have prismatic tips, although many grains are broken (Supplemental File 2 in Supporting Information S2). Forty

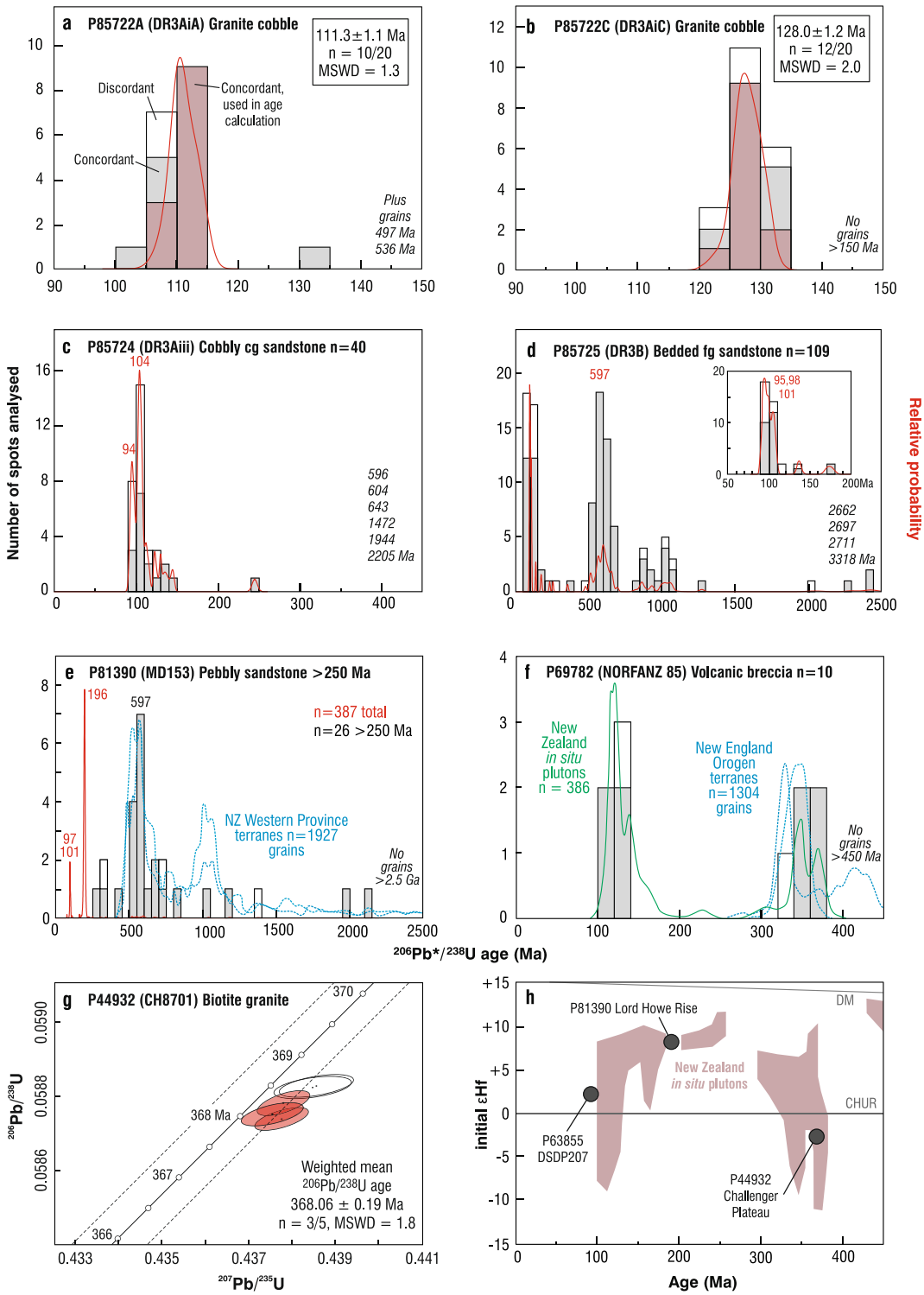


**Figure 5.**

zircon grains were not spilled on the laboratory floor by the senior author and were subsequently dated. Two thirds of the zircons are Early Cretaceous (Figure 5c) with statistical populations of 94 and 104 Ma. Individual zircon ages span a broad Early Cretaceous age range similar to the two granitoid clasts; the 94 Ma peak is distinctly younger (but is based on only three zircons). Eight percent of the grains ($n = 3$) have ages in the range 700–500 Ma. The high proportion of volcanic lithic grains in P85724 means that a contributor of zircons could

be siliceous volcanic rocks. The seven pre-200 Ma zircon grains are no different in shape or cathodoluminescence from the Cretaceous zircons (Supplemental Files 2 and 3 in Supporting Information S2).

Zircon grains in the better-sorted and finer-grained quartzofeldspathic sandstone slab, P85725, are a mix of euhedral, broken, and rounded shapes. Like P85724, many zircon grain $^{206}Pb/^{238}U$ ages range from 115 to 90 Ma, and most contribute to a statistical peak at 95 Ma (Figure 5d inset). The main difference between the two sandstones is that, remarkably, two thirds of the zircons in P85725 are older than 500 Ma (Figure 5d). Within these >500 Ma zircons, groupings of 700–500 Ma (= 42% of ages) and 1,100–800 Ma old zircons can be identified. There is no relationship between age and rounding, with both euhedral and rounded grains noted in Cretaceous and Cambrian age populations.

#### 5.2.2. Lord Howe Rise and Challenger Plateau

P81390 is a pebbly sandstone from the central Lord Howe Rise (Figure 1). Ages of 94 euhedral to subhedral zircon grains from this rock were first reported by Mortimer et al. (2015). They indicated an imprecise Late Cretaceous depositional age for the sandstone, whose content was dominated (89%) by Late Triassic to Early Jurassic zircon grains with a statistical $^{206}Pb/^{238}U$ age peak at 196 ± 1 Ma. Four grains were pre-Triassic. To extract further age information from this sample especially of the older grains, we obtained a further 293 U-Pb ages from P81390 that were <10% discordant (Figure 5e, Supplemental File 4 in Supporting Information S2). The combined data set of 387 dated grains confirms the approximate age proportions of Mortimer et al. (2015) namely 10% Cretaceous, 83% Triassic-Jurassic and 7% pre-Triassic (Figure 5e). We also confirm the previously established dominant 196 Ma age peak for the sandstone. In the expanded data set, statistical age peaks of 97 and 101 Ma are now evident. Although there are only 26 pre-Triassic grains, seven define a statistical peak at 597 Ma but otherwise are spread between 2,133 and 251 Ma. All pre- and post-Triassic-Jurassic ages are from discrete detrital grains; there are no older core or younger rim relationships.

P69782 is a volcanic breccia from the southern Lord Howe Rise (Figure 1) in which a tiny fraction of the granule-sized clasts are schist and greywacke (Mortimer et al., 2008). Using Sr and Nd isotopic ratios of the schist and greywacke clasts, Mortimer et al. (2008) correlated them with metasedimentary terranes of the New England Orogen. To test this interpretation, we extracted zircon from the bulk breccia and were able to date 10 grains (Figure 5f; Supplemental File 5 in Supporting Information S2). Two age clusters are present. Five grains lie in the range 130–119 Ma and five in the range 373–359 Ma (or to 336 Ma if a discordant grain is included). There are too few grains to define statistical peaks.

A sample of granite basement (sample P44932) dredged from the western margin of the Challenger Plateau was previously analyzed by legacy multi-zircon U-Pb ID-TIMS methods and yielded a lower concordia intercept age of 335 ± 7 Ma Tulloch et al. (1991). Based on its age and geochemistry, this granite was linked to the predominantly Devonian S-type granites of the (then very broadly defined) Karamea Suite. Five new high-precision single-zircon CA-ID-TIMS analyses from the same P44932 mineral separate of Tulloch et al. (1991) exhibit a spread in $^{206}Pb/^{238}U$ ages from 367.95 ± 0.19 to 368.49 ± 0.19 Ma (Figure 5g, Supplemental File 6 in Supporting Information S2). We interpret the youngest three overlapping analyses to reflect the age of granite crystallization. The weighted mean $^{206}Pb/^{238}U$ age of these three youngest zircon grains is 368.06 ± 0.19 Ma (MSWD = 1.8). This is substantially older than the reported legacy age and overlaps with a pulse of magmatism within the high flux (and now more narrowly defined) 370-368 Ma Karamea Suite "flare-up" event (Turnbull et al., 2016). The high-precision U-Pb CA-ID-TIMS age is supported by a less precise LA-ICP-MS weighted mean $^{206}Pb/^{238}U$ zircon age of 371.1 ± 3.8 Ma (MSWD = 3.0) (Supplemental File 7 in Supporting Information S2).

### 5.3. Hf and O Isotope Zircon Data

Hafnium isotope data were collected for 35 zircon grains from the central Lord Howe Rise plutoniclastic sandstone P81390. The grains had ages between 194 and 183 Ma (Early Jurassic). The range of initial εHf values

**Figure 5.** U-Pb zircon ages and zircon Hf isotope data. Red lines are Gaussian-summation probability density distributions for dated samples plotted with stacked column histograms. (a) Fairway Ridge granite cobble P85722A (DR3AiA); concordant grains not used in age calculation have lost Pb or are inherited. (b) Fairway Ridge granite cobble P85722C (DR3AiC); concordant grains not used in age calculation have lost Pb or are inherited. (c) Fairway Ridge coarse-grained sandstone matrix P85724 from which cobbles were extracted (DR3Aiii). (d) Fairway Ridge bedded fine-grained sandstone P85725 (DR3B) (e) Central Lord Howe Rise plutoniclastic pebbly sandstone P81390 (Mortimer et al., 2015). Note the probability density distribution in panel (e) is for the entire 387 grains but the histogram is vertically stretched to show only the 26 grain ages older than 250 Ma. (f) Southern Lord Howe Rise volcanic breccia P69782 (Mortimer et al., 2008). Reference terrane probability density distributions (blue lines) from Adams et al. (2015) and Korsch et al. (2009), reference pluton age probability density distribution (green line) from Ringwood et al. (2021). (g) Challenger Plateau granite P44932. (h) Initial Hf isotope plot. DSDP207 data from van der Meer et al. (2018), reference in situ New Zealand pluton field from data in Nebel et al. (2007) and Turnbull et al. (2023); reference lines: DM = depleted mantle and CHUR = chondritic uniform reservoir.

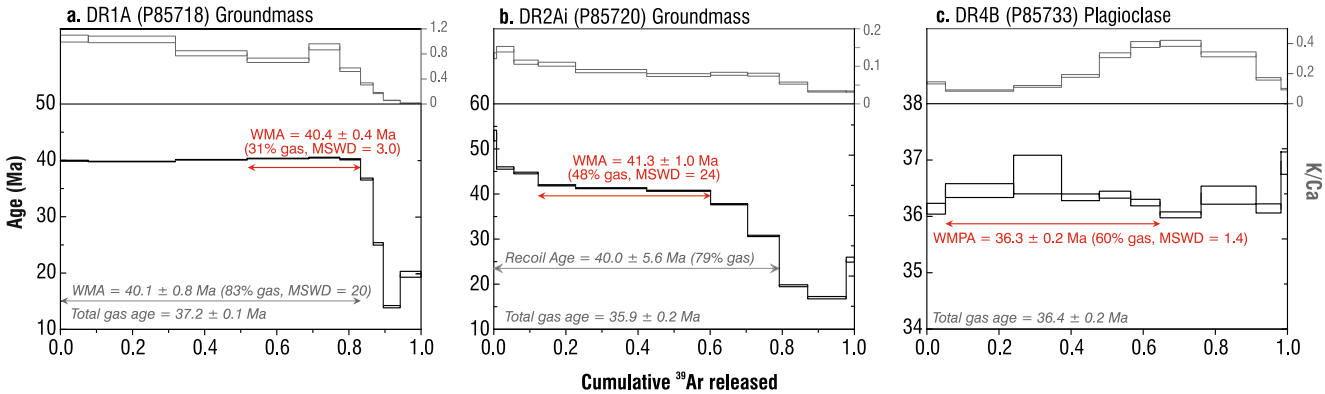


**Figure 6.** IN2016T01 Ar-Ar spectra. (a) DR1A nephelinite groundmass (P85718). (b) DR2Ai basanite groundmass (P85720). (c) DR4B doleritic basalt plagioclase (P85733). WMA = weighted mean age and WMPA = weighted mean plateau age. Boxes are ±1σ in height but labeled ages are ±2σ.

is +13.2 to +5.2, with the mean and median values being +8.3 and +8.1 respectively (Supplemental File 4 in Supporting Information S2). The initial εHf values are within the range of plutons emplaced in the eastern part of the Median Batholith which are derived from relatively juvenile and/or mantle-like sources with limited involvement of older crust (Figure 5h, Schwartz et al., 2021; Turnbull et al., 2023). These initial εHf values are also within the range of New Zealand detrital zircons interpreted to have been derived from the Median Batholith arc (Campbell et al., 2020) and have substantially higher initial εHf than the +2.6 median (+2.3 mean) reported for 35 zircons from the 97 Ma rhyolite at DSDP 207 (Figure 1) by van der Meer et al. (2018).

Challenger Plateau granite zircons have median $\delta^{18}O = 9.2 \pm 1.9‰$ ($n = 10$), and median initial $\varepsilon Hf = -2.5 \pm 3.2$ (2σ error, $n = 18$) (Supplemental File 7 in Supporting Information S2). The Challenger Plateau granite O and Hf isotope values overlap those established for New Zealand's Karamea Suite in Turnbull et al. (2023) (Figure 5h).

### 5.4. Ar-Ar Geochronology

Five basaltic samples from the Fairway Ridge were dated by Ar-Ar methods, in part to confirm and/or improve on the micropaleontological dating of the IN2016T01 DR1 and DR2 samples reported by Mortimer et al. (2019). The results of the dating of the samples from DR1 and DR2, and the best result of three dated samples from DR4 are shown in Figure 6 (see also Supplemental File 8 in Supporting Information S2). The degassing spectrum of the DR1A (P85718) nephelinite groundmass shows a mostly flat pattern for much of the gas release but the steps do not quite form a statistically valid plateau. As the best age from P85718, we use three steps (31% of gas) which give a weighted mean age of 40.4 ± 0.4 Ma (±2σ error) and an MSWD of 3.0 (Figure 6a); an alternative interpretation is a six-step age (83% of gas) of 40.1 ± 0.8 Ma with an MSWD of 20. The degassing spectrum of groundmass from DR2A (P85720) basalt shows a classic recoil pattern of older ages in the low temperature steps, descending to a mostly flat set of steps, with ages decreasing still further at the highest temperature release. As the best age for this rock, we use the weighted mean of three of the mostly flat steps (48% of gas) which give an age of 41.3 ± 1.0 Ma (Figure 6b). This is the least precise of our three reported ages, and is slightly older than, but just within error of, P85718. Groundmass age spectra of two basaltic samples (P85731, 32) from DR4 show disturbed hump-shaped spectra (Supplemental File 8 in Supporting Information S2) with low confidence age interpretations of 36–34 Ma. However, as the best and representative age of the three petrologically related samples from DR4, we use the weighted mean plateau age of five steps (60% gas) from P85733 plagioclase, namely 36.3 ± 0.2 Ma (Figure 6c). The seemingly more irregular spectrum in Figure 6c is simply due to the expanded *y*-axis scale. In summary, three dated alkaline intraplate mafic lavas from three sites on the Fairway Ridge are 41–36 Ma (Middle to Late Eocene) in age.

### 5.5. Rb-Sr Dating

Strontium isotope data were obtained for three volcanic clasts from IN2016T01 DR3, mainly to assess their petrological character and to explore crustal contamination in their petrogenesis (Figure 4f). However, we additionally used the isotopic data on an Rb-Sr isochron diagram to give age information (Figure 7). The volcanic clasts

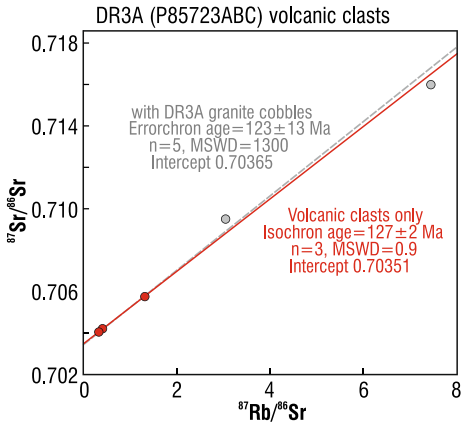


**Figure 7.** Rb-Sr isochron plot of IN2016T01-DR3 andesite, dacite, and rhyolite cobbles (P85723B, A and C respectively). Fairway Ridge granite cobble points shown for reference. Best fit lines calculated using errors of 0.2% for Rb/Sr and 0.003% for $^{87}Sr/^{86}Sr$ (Borst et al., 2018).

define an isochron of slope 127 ± 2 Ma. Two points have very similar isotope ratios, so the age is poorly defined, being basically a two-point isochron. If the Rb-Sr isotope data for the two DR3 granite cobbles are also included (on the basis that they could be the same igneous suite) the best fit line for all five DR3 clasts has a slope indicating an age of 123 ± 13 Ma (Figure 7); the very high MSWD indicates this is an errorchron.

### 5.6. Regional Magnetic Data

Continental North Zealandia has a textured magnetic relief with anomalies of variable orientation, wavelength, and amplitude (Figure 8). The two most prominent magnetic features are a pair of subparallel positive linear magnetic anomalies, labeled C1 and C2 in Figure 8, which are present on either side of the southern New Caledonia Trough (compare with bathymetry in Figure 1). C1 and C2 are some of the highest (>1,000 nT) anomaly values in the entire Zealandia continent. Their presence has previously been noted by several surveys and compilations including those by Davy (1991), Sutherland (1999), and Collot et al. (2009). North of 31°S another pair of anomalies, labeled F1 and F2 in Figure 8, are co-linear with C1 and C2 and lie within the Lord Howe Rise. F1 and F2 mark the edges of the Fairway Basin, with F2 coincident with the Fairway Ridge (Collot et al., 2009). Along the northern edge of North Zealandia, a strong linear positive anomaly, R in Figure 8, strikes NE-SW and coincides with the Coriolis Ridge of Exon et al. (2006b). Anomaly R is not a bent or rotated continuation of F1 or F2 but is a separate feature.

West and south of C1 and F1 short and discontinuous linear ~200–300 nT positive magnetic anomalies are present. Many of these are parallel and/or perpendicular to the strike of identifiable rift trends such as the New Caledonia Trough, Fairway Basin, Coriolis Ridge, and the Zealandia-Tasman Sea Basin continent-ocean boundary. Elsewhere, more equant positive magnetic anomalies are scattered across North Zealandia, some in distinctive belts, such as along and near the eastern edge of North Zealandia (Figure 8).

## 6. Discussion

The acoustic basement of North Zealandia has been imaged in many seismic reflection projects (e.g., Bache et al., 2012; Collot et al., 2023; Gallais et al., 2019; Higgins et al., 2015; Klingelhoefer et al., 2007). In most cases, the isotropic and diffractive nature of acoustic basement indicates the presence of widespread crystalline basement (plutonic, metamorphic and/or complexly deformed sedimentary and/or volcanic rocks). However, sporadically observed intra-basement reflectors suggest the presence of some sub-horizontally bedded sedimentary terranes (e.g., Bache et al., 2012; Collot et al., 2023; Klingelhoefer et al., 2007). Given the variability in quality of seismic surveys, and variable thickness of sedimentary basins we have not used seismic character to map North Zealandia basement (but see Section 6.1.2 below).

In terms of data quality, quantity and spatial extent, Mesozoic arc rocks are the most useful in defining basement geological trends across North Zealandia (Figure 9). The components of the Mesozoic orogen are discussed first, followed by other features.

### 6.1. Mesozoic Orogen

#### 6.1.1. Magmatic Arc

In onland New Zealand, autochthonous subduction-related plutonic suites of Triassic to Early Cretaceous age all lie within the Median Batholith and/or within the metasedimentary rocks of the adjacent Western Province (e.g., Mortimer et al., 1999, 2014a, 2014b; Ringwood et al., 2021). At the scale of Figure 9 the batholith and associated plutons are almost superimposed and collectively mark the location of a long-lived subduction-related continental magmatic arc that formed along the margin of South Gondwana. Three Median Batholith I-type suites are relevant to this paper: the 265–245 Ma Longwood Suite, 235–135 Ma Darran Suite and 130–105 Ma Separation Point Suite (Mortimer et al., 2014a, 2014b and references therein). The Mesozoic arc has been mapped

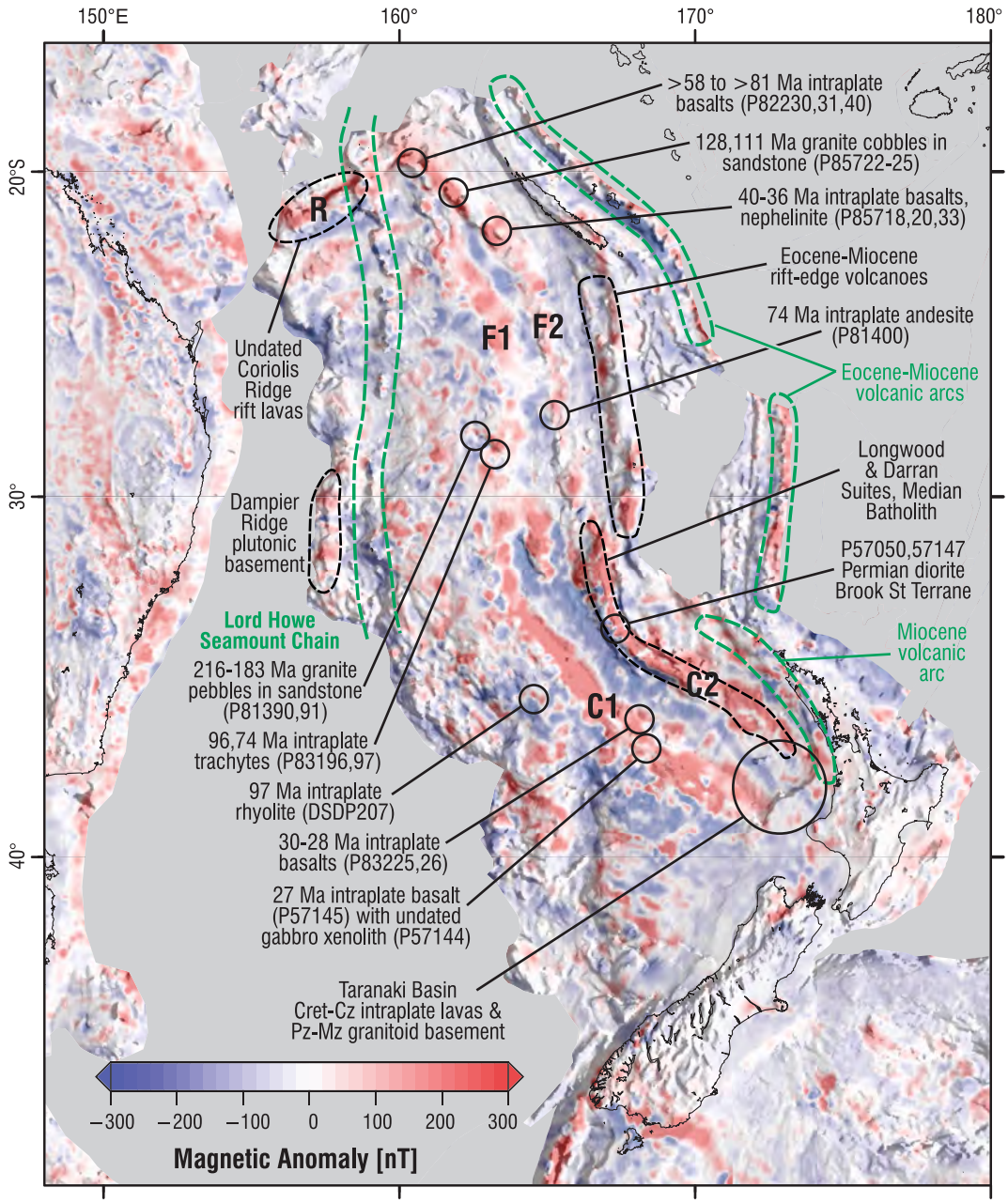


**Figure 8.** EMAG2 total magnetic intensity anomalies of North Zealandia and adjacent continental regions (Meyer et al., 2017), draped on east-illuminated digital terrain model. Oceanic and backarc basin crust is masked. Major continental anomalies are labeled (see text for discussion). Rock sample ground truth data (black labels) from Mortimer (2004), Exon et al. (2006b), Mortimer et al. (1997, 1998, 2018), Uruski (2020), and this study. Green labels indicate other general geological information from McDougall et al. (1994), Seton et al. (2019), and Gans et al. (2023).

across South Zealandia and was formerly contiguous with a Mesozoic magmatic arc in West Antarctica (Tulloch et al., 2019).

With the progressive acquisition of new samples and their analysis, Triassic-Early Cretaceous Median Batholith arc rocks have been progressively mapped across North Zealandia from its onland exposures in New Zealand's South Island at ~41°S. Mortimer et al. (1997) dated and traced Mesozoic plutons in the offshore Taranaki Basin near 39°S. Mortimer et al. (1998) reported a 247 Ma granodiorite, a 146 Ma gabbrodiorite, and a 117 Ma granite from the West Norfolk Ridge at ~34°S. The 196 Ma detrital zircon sandstone age peak and 216–183 Ma granite pebbles in the Lord Howe Rise MD153-DR01 dredge extrapolated the extent of the Mesozoic arc to ~29°S

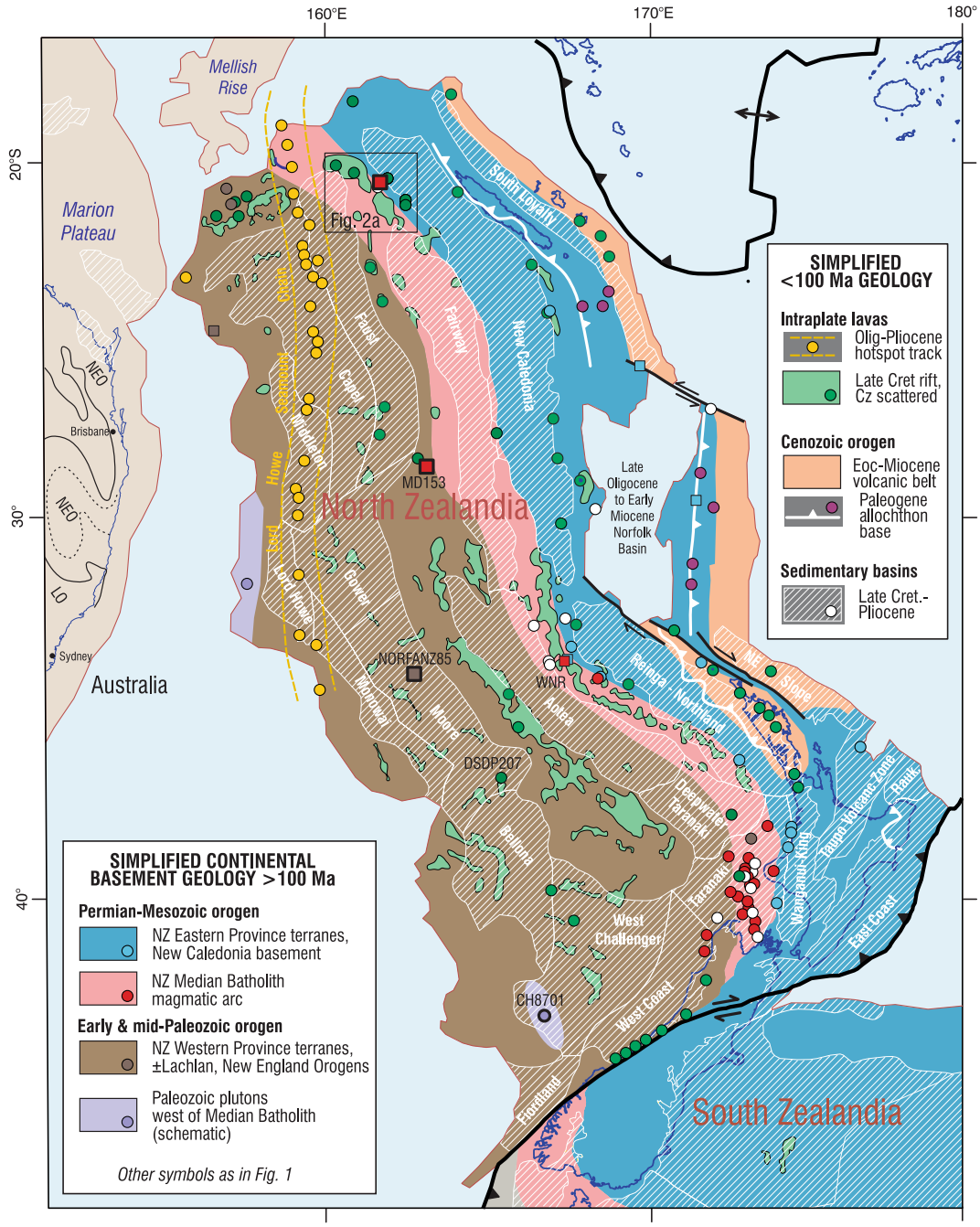


**Figure 9.** Simplified basement geology of North Zealandia based on sources mentioned in the text, Mortimer, Smith Lyttle, and Black (2020), and this study. Sedimentary basin names in white text, extent of sedimentary basins not shown beyond continental crust. LO = Lachlan Orogen and NEO = New England Orogen.

(Mortimer et al., 2015). In this paper we have identified granite cobbles and volcanic pebbles from the Mesozoic arc in the new IN2016T1-DR3 Fairway Ridge dredge near 20°S.

We tentatively interpret the stratigraphic age of the Fairway Ridge DR3 pebbly cobbly sandstones to be 95–94 Ma based on the minimum detrital zircon age peak of the two samples. As mentioned in Section 5.1, the age, geochemical and isotope data of the Fairway Ridge DR3 granite cobbles point to an Early Cretaceous continental magmatic arc source similar to New Zealand Mesozoic plutonic suites. The Sr and Nd isotopic data and paucity of inherited zircon in the granite cobbles indicates negligible to minimal involvement of old continental crust

in their petrogenesis. The Fairway Ridge DR3 volcanic cobble compositions lie within Darran and Separation Point Suite igneous fields (Figures 4e and 4f). As do the compositions of the lithic-rich (lower $SiO_2$) sandstones (Figures 4b, 4d, and 4e). The Rb-Sr isochron diagram for the DR3 volcanic clasts (Figure 7) tentatively supports an Early Cretaceous age for these lithologies. However, because of the limited Rb/Sr ratio of the samples, and uncertainties in whether they are part of a single volcanic-stratigraphic succession and whether the Sr isotope system has remained closed since the time of eruption, the age assignment is no more than indicative. Assuming the granite and volcanic cobbles traveled at most 10–100 km, we position the arc to lie within ∼100 km of the Fairway Ridge. No in situ Jurassic to Early Cretaceous igneous rocks are exposed in New Caledonia; the basement there comprises late Paleozoic to Mesozoic forearc basin and accretionary wedge terranes (Maurizot et al., 2020a). The provisional location of the Mesozoic arc is shown in pink in Figure 9.

We acknowledge it is less than satisfactory to have to track the location of a basement rock unit using recycled clasts rather than in situ samples. However, Adams et al. (2017) found that the detrital zircon provenance of most Late Cretaceous non-marine and marine sandstones in New Zealand commonly matched those of local basement, rather than being well-mixed across and between sedimentary basins. Other lines of evidence that support the Mesozoic arc being located on or near the Fairway Ridge include the commonly cited structural co-linearity of the basement highs of the Fairway Ridge and West Norfolk Ridge (e.g., Collot et al., 2009), and the preservation of approximately the same Mesozoic arc-trench gap along the entire edge of North Zealandia, as indicated by the constant lateral distance from the arc to the pre-Cenozoic eastern edge of the continent (Figure 9).

The inferred width of the Mesozoic batholithic arc in North Zealandia is uncertain but, like Tulloch et al. (2019), we schematically draw it wider than its onland New Zealand width where oroclinal bending has likely trimmed and thinned it. Because of lateral migration, long term (>10 Myr) continental magmatic arc footprints are substantially broader than instantaneous volcanic arc chains and can be 250–650 km wide (Ducea et al., 2015).

In this paper, we do not explore the projected continuation of the Mesozoic arc into the Australian continent or the Mellish Rise (Figure 9). The location of a 145–140 Ma arc in coastal Queensland has been proposed by Henderson et al. (2022) but, as inferred by Bryan et al. (2000) and Bryan and Purdy (2013), much Early Cretaceous magmatism in onland Queensland is probably of continental back-arc or intraplate nature. The main Early Cretaceous arc footprint probably lies, thus far unsampled, somewhere under the Mellish Rise or Marion Plateau.

#### 6.1.2. Eastern Province Forearc and Accretionary Wedge

In New Zealand, the Median Batholith is so named because it occupies a medial position between tectonostratigraphic terranes of the Eastern and Western Provinces (Mortimer et al., 1999, 2014a, 2014b). Eastern Province terranes represent fore-arc and accretionary wedge assemblages spatially related to the Median Batholith arc (Mortimer et al., 2014a, 2014b).

Eastern Province greywackes have been drilled in eastern Taranaki Basin boreholes and dredged from West Norfolk, Wanganella, and Reinga Ridges, and from Colville Knolls (Figures 1 and 9, Mortimer et al., 1997, 1998, 2009; Mortimer, Adams, & Wright, 2020). The greywackes and schists of the Téremba, Koh-Central and Boghen Terranes of New Caledonia (Maurizot et al., 2020a) are a Mesozoic accretionary assemblage and can be considered Eastern Province equivalents. Xenoliths of probable quartz veins were found in a lava dredged from the northern Norfolk Ridge (Mortimer et al., 2021). Detrital zircon grains of Permian to Cretaceous age, likely sourced from Eastern Province basement, have been obtained from Late Oligocene sedimentary rocks on the Three Kings and Loyalty Ridges (Figures 1 and 9, Crawford, 2004; Gans et al., 2023; Meffre et al., 2006).

Seismic reflection profiles are generally of more use in outlining sedimentary basins than in subdividing or defining crystalline basement units (Section 6.5). However, intra-basement seismic reflectors under the Reinga Basin, Norfolk Ridge and southern New Caledonia Trough have previously been correlated with the generally flat-lying Murihiku Terrane fore-arc basin strata of the Eastern Province (Bache et al., 2012; Collot et al., 2023; Uruski, 2023). Collectively the sample and seismic data support the case that Eastern Province terranes and their equivalents underlie the entire eastern basement of North Zealandia.

### 6.2. Paleozoic Orogen

#### 6.2.1. Paleozoic Plutons

Pre-Triassic plutonic rocks have been sampled west of the Mesozoic arc (Figure 9). These are the Devonian Challenger Plateau granite (Tulloch et al., 1991; this study) and Carboniferous to Permian plutonic rocks on

the Dampier Ridge (McDougall et al., 1994). The new 368 Ma age, high initial $^{87}Sr/^{86}Sr$ ratio, and zircon O and Hf isotope values of the Challenger granite can be confidently matched with the S-type Karamea Suite of New Zealand. While the Paleozoic plutonic suites of Zealandia have some correlatives in the Lachlan Orogen (i.e., Devonian plutons in the Melbourne Zone), they appear more strongly correlated to Paleozoic plutonism in Tasmania (Glen & Cooper, 2021; Turnbull et al., 2016). The 95 Ma K-Ar sericite age of P44932 was attributed by Tulloch et al. (1991) to rift-related hydrothermal alteration.

In contrast, the Dampier Ridge rocks have no plutonic equivalents in New Zealand and have I-type isotopic characteristics which McDougall et al. (1994) compared with the Nundle Suite of the New England Orogen. We regard it as premature to try to map the extent of Paleozoic Gondwana margin arcs from just the two Challenger Plateau and Dampier Ridge dredges. Therefore, they are shown simply as schematic blobs in Figure 9.

#### 6.2.2. Western Province Gondwana Basement Terranes

Western Province terranes mostly comprise quartz-rich (siliceous) greywackes and schists with dominantly Cambrian to Ordovician protolith ages (Cooper & Tulloch, 1992; Mortimer et al., 2014a, 2014b; Roser & Korsch, 1986 and references therein). By the Mesozoic, these terranes represented autochthonous (previously accreted) Gondwana basement. New Zealand Western Province terranes are commonly correlated with the Lachlan Orogen of Australia (e.g., Cooper & Tulloch, 1992; Glen & Cooper, 2021). The Early Paleozoic terranes of the Western Province and Lachlan Orogen typically contain large proportions of late Precambrian-Cambrian (700–500 Ma) detrital zircon grains (Adams et al., 2015; Ireland & Gibson, 1998). This detrital zircon signature contrasts with terranes of the New England Orogen which are dominated by Devonian and Carboniferous protoliths and detrital zircon populations (Shaanan et al., 2018).

In offshore North Zealandia, siliceous greywackes and schists were intersected in a central Taranaki Basin borehole within the Median Batholith and were correlated with Western Province rocks (Figures 1 and 9, Mortimer et al., 1997). Undated meta-quartzites and quartz-rich sandstones were reported from dredges on the Selfridge Rise and Kenn Plateau by Exon et al. (2006b). Our new U-Pb dating of 26 xenocrystic zircon cores from the matrix of the Late Cretaceous MD153 granitic pebbly sandstone reveals ages that are significantly older than the 196 Ma age of the granite clasts. The ∼597 Ma (Late Neoproterozoic) zircon age peak (Figure 5e) matches that found in New Zealand Western Province greywackes (Adams et al., 2015). The older zircon ages indicate that the MD153 Early Jurassic granite(s) probably intruded Western Province host rocks and that the Median Batholith-Western Province boundary can plausibly be drawn close to the MD153 dredge site (Figure 9).

The two dated Late Cretaceous IN2016T1 DR3 Fairway Ridge sandstones also contain 700–500 Ma detrital zircon populations. These comprise only ∼8% of the 40 dated grains in the coarse-grained sandstone but 42% in the fine-grained sandstone (Figures 5c and 5d). Additionally, 14% of the zircons in the fine-grained sandstone are 1,100–800 Ma; this "tail" of older Precambrian zircons also fits with Western Province sources (Adams et al., 2015). As with the reasoning for MD153 above, these Late Precambrian populations point to a New Zealand Western Province (or an Australian Lachlan Orogen) source area rather than a Median Batholith source. Some provenance switching is indicated between the two DR3 sandstones: P85725 is a fine-grained arkosic petrofacies dominated by a Precambrian zircon population whereas P85724 is a coarse-grained lithic petrofacies dominated by Cretaceous plutoniclastic and volcaniclastic zircons.

Scant zircons from the NORFANZ85 volcanic breccia dredged from the southern Lord Howe Rise are 130–119 and 373–359 Ma in age (373–336 Ma if an analytically discordant grain is included) (Figure 5f). This Paleozoic zircon age range is different from the MD153 (P81390) and Fairway Ridge samples (Figure 5). The small number of grains dated means that caution should be exercised. We note that the while the NORFANZ85 Devonian ages are similar to detrital zircon ages of sedimentary rocks of the New England Orogen (Figure 5f, Korsch et al., 2009; Shaanan et al., 2018), they perhaps better match a major pulse of New Zealand plutonism (Figure 5h, Ringwood et al., 2021). Yet, because the breccia contained small greywacke and schist xenolithic clasts (Mortimer et al., 2008), it might be presumed that the Paleozoic zircons came from metasedimentary rather than plutonic rocks. Based on Sr and Nd isotope ratios of the clasts, Mortimer et al. (2008) interpreted a New England Orogen, rather than a Western Province, origin for the breccia clasts. Our dating of 10 zircons from the breccia (Section 5.2.2) loosely supports this earlier New England Orogen interpretation but also raises the possibility that the NORFANZ85 zircons were sourced from correlatives of New Zealand Cretaceous and Paleozoic plutonic suites.

In summary, of the four places in North Zealandia where information can potentially be obtained on meta-sedimentary basement west of the Mesozoic arc, three (Taranaki Basin, MD153, and Fairway Ridge) point to New Zealand Western Province sources and one (NORFANZ 85) to a New England Orogen source. At face value, this complicates the map pattern of Mortimer et al. (2008) in which the Western Province and Lachlan Orogen always lie west of the strike of the New England Orogen. There are confounding factors in trying to draw Paleozoic orogen trends across North Zealandia: (a) the MD153 and Fairway Ridge 700–500 Ma detrital zircons need not have been sourced from local New Zealand Western Province basement. They could have been transported in Cretaceous rivers from a distant Lachlan Orogen in Australia and/or been released from Permian continental basin strata which could have underlain (and could still underlie) large parts of North Zealandia (cf. Adams et al., 2022) and (b) 100 km-scale oroclinal bends are present in the onland Australia Lachlan and New England orogens (Figure 9, Rosenbaum, 2018) and raise the possibility of strike change complexities across North Zealandia. As such, until further samples clarify the situation, we do not attempt to map separate Western Province-Lachlan and New England orogens across North Zealandia in this paper.

### 6.3. Cenozoic Orogen

A distinctive feature of the eastern margin of North Zealandia is the presence of ophiolitic allochthons which are absent from South Zealandia. Ophiolite massifs are major physiographic features of onland North Island New Zealand and New Caledonia (Isaac et al., 1994; Maurizot et al., 2020b). For the most part the allochthons comprise west-directed low-angle faults, emplaced in the Eocene and Oligocene, with igneous crust and mantle rocks forming the uppermost sheets. The submarine extent of the ophiolitic sheets southeast of New Caledonia was traced in seismic lines by Patriat et al. (2018), ground-truthed by serpentinite, pyroxenite and tonalite rock dredges (Mortimer et al., 2014a, 2014b). Closer to New Zealand, dredges of peridotite on the Three Kings Ridge (Crawford, 2004) and seismic interpretations near the North Island (Herzer et al., 2009; Orr et al., 2020) have allowed delineation of this offshore part of the allochthon. The western limits of the overlying allochthons between New Caledonia and New Zealand are shown in Figure 9 by toothed white lines.

Allochthon emplacement in New Zealand was followed immediately by subduction related (arc) volcanism (Isaac et al., 1994). An Eocene subduction-related volcanic arc is inferred to underlie the Loyalty Ridge (Collot et al., 2011; Maurizot et al., 2020b and references therein). Linking these two areas, a belt of arc and backmost-arc volcanic rocks of Eocene to Miocene age has recently been sampled and mapped along most of the eastern edge of North Zealandia (Gans et al., 2023) and is shown in Figure 9. The spatial coincidence of the volcanic arc with the ophiolitic allochthons is probably no coincidence, the two both being responses to Cenozoic subduction initiation along the northeastern edge of Zealandia (Sutherland et al., 2020).

### 6.4. Intraplate Volcanic Rocks

#### 6.4.1. Lord Howe Seamount Chain

The Lord Howe Seamount Chain (yellow symbols on Figure 9) is interpreted as an Oligocene-Pliocene age-progressive hotspot track that records the northward movement of the Australian Plate lithosphere (Mortimer et al., 2018; Rogers et al., 2023; Seton et al., 2019). Apart from the large guyots at its northern end, the Lord Howe Seamount Chain has minimal magnetic expression, with the age-progressive seamounts marked by small positive anomalies less than 30 km across.

#### 6.4.2. Rift and Other

One of the main contributions of the Tulloch et al. (2019) paper on South Zealandia was the novel identification of a widespread syn-Gondwana breakup mafic igneous province, mapped using >200 nT rectilinear positive magnetic anomalies. This was supported by four main lines of evidence: (a) shape of some anomalies being parallel and/or perpendicular to known extensional rift structures, especially the continent-ocean boundary; (b) interpretation and modeling of some of the Campbell Plateau anomalies by Grobys et al. (2009) as mafic igneous underplates and shallow crustal dike-like bodies; (c) ground-truthing of one of the positive magnetic anomalies with Late Cretaceous intraplate lavas in the Chatham Islands; and (d) general lack of magnetic expression of the onshore Median Batholith Mesozoic magmatic arc; previously, this arc was invoked by Grindley and Davey (1982) and Sutherland (1999) as the cause of the Campbell Magnetic Anomaly System.

There are at least eight places in North Zealandia where rectilinear positive magnetic anomalies C1, C2, F1, F2, and R have been ground-truthed as being caused by sampled intraplate igneous rocks (Figure 8). The strongest positive anomalies coincide with basement highs where sedimentary basins are absent. As with South Zealandia, age control from direct sampling is limited. The positive anomalies coincide with volcanic rocks dated from Late Cretaceous to Miocene (Figure 8). The length of the Cretaceous Normal Superchron (~126–84 Ma) gives ample time in which to intrude and/or erupt igneous rocks. The widespread occurrence of detrital zircons of 101–94 Ma age in North Zealandia dredges (Figures 6c–6e; Mortimer et al., 2010, Figure 4a) could be attributed to distributed eruptions of Late Cretaceous siliceous igneous rocks. Relief on Zealandia's lithosphere-asthenosphere boundary dating from the Late Cretaceous could have induced asthenospheric shear disturbances and melting throughout the Cenozoic (cf. Farrington et al., 2010). Locally, rifting directions have been extracted from Lord Howe Rise basins (e.g., Higgins et al., 2015). Collectively, these observations give us confidence to use the +200 nT contour around rectilinear areas in a comparable way to Tulloch et al. (2019), to map the location of Late Cretaceous to Paleogene rift-related igneous rocks, at least schematically (Figure 9, green blobs). The linear shape of the C1, C2, F1, F2, and R anomalies and association with bathymetric relief (e.g., New Caledonia Trough, Coriolis Ridge) emphasize a faulted rift edge control of these volcanic rocks more so than for South Zealandia.

Davy (1991) commented that the C1 and C2 anomalies were not simply edge effects from sheets either side of the New Caledonia Trough. Lapouille (1977) modeled the F2 Fairway Ridge anomaly as a downward widening, highly magnetic body extending to at least 10 km below sea level. Frey (1985) and Schreckenberger et al. (1992) noted that the crust of the Challenger Plateau and Lord Howe Rise is, on balance, more magnetic than would be expected for simple thinned continental crust. They invoked the presence of dispersed and/or underplated mafic igneous rocks to account for these features, an interpretation that fits with our own one of widespread volumes of rift-related igneous rocks (cf. South Zealandia underplates and intrusions of Grobys et al., 2009). In the case of anomaly C2 (Figure 8), the >200 nT anomalies are possibly amplified or primarily caused by magnetic Late Permian-Early Triassic Longwood Suite gabbros of the Median Batholith (Mortimer et al., 1998; Sutherland, 1999).

Not all magnetic anomalies in Figure 8 are rectilinear. Using onland geology maps and offshore sub-circular bathymetric, gravity and magnetic anomalies, Mortimer and Scott (2020) identified more than 500 volcanoes across North and South Zealandia that were not obviously rift-related. Many other non-linear, short wavelength positive magnetic anomalies in Figure 8 most likely result from scattered intraplate mafic volcanic rocks exposed on or close to the seabed. Some of these have been confirmed by drilling or dredging (e.g., Mortimer et al., 1998, 2018), while buried ones have been imaged in seismic reflection profiles (e.g., Uruski, 2020).

### 6.5. Sedimentary Basins

North Zealandia has a cargo of Late Cretaceous to Pliocene sedimentary basins, draped on the aforementioned older crystalline basement (e.g., Figure 2c). The outline of the basins in Figure 9 is derived from syntheses of large numbers of seismic reflection profile surveys for example, Stagg et al. (1999), Norvick et al. (2008), Collot et al. (2009), Sutherland et al. (2012), Higgins et al. (2015), Arnot and Bland (2016), and Uruski (2020, 2023). Intraplate and subduction-related lavas (Sections 6.3 and 6.4) are interbedded with the sedimentary rocks. Interpretations of at least parts of the New Caledonia and Middleton Basins being underlain by small areas of atypically thick oceanic crust have been presented by Klingelhoefer et al. (2007) and Gallais et al. (2019). For this paper, we adopt the position that all sedimentary basins in Figure 9 are just as likely to be underlain by intruded and thinned to hyperextended continental crust—similar to interpretations of Riefstahl et al. (2020) in South Zealandia. The location of Zealandia's continent-ocean boundary is particularly complex and uncertain in the Norfolk Basin.

### 6.6. Reconstruction of Gondwana at ~100 Ma

There have been many reconstructions of New Zealand and Zealandia against Australia, using geological similarities and correlations between these two continents (e.g., Cooper & Tulloch, 1992; Gaina et al., 1998; Griffiths, 1971; Grindley & Davey, 1982; Mortimer et al., 2008; Strogen et al., 2022; Sutherland, 1999). However, at a continental scale, most of these employ rigid block reconstructions that do not attempt to unstretch the now thinned and submerged crust of Zealandia. Therefore, these unstretched paleo-reconstructions have unrealistically exaggerated bulges in the Gondwana continent-ocean boundary and show artificial fault-like offsets and gaps

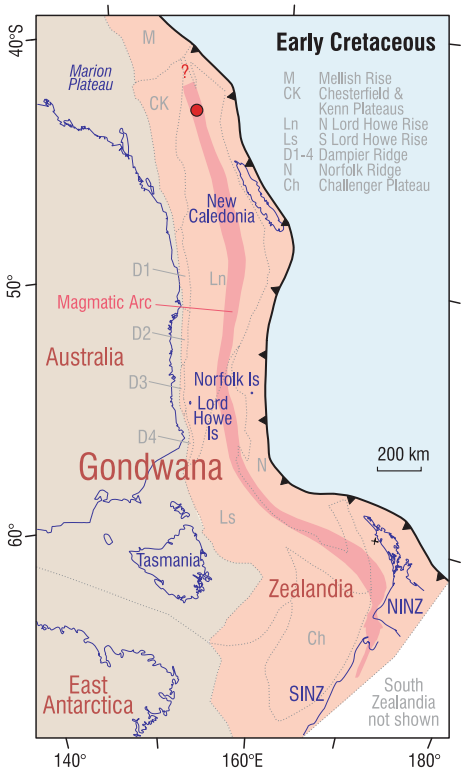


**Figure 10.** Early Cretaceous reconstruction of North Zealandia against eastern Australia using GPlates and a continuous deforming mesh. Gray dotted lines and letters are rigid blocks used by Gaina et al. (1998). Marion Plateau, Challenger Plateau, and North Island New Zealand have not been retrodeformed.

between rigid crustal blocks. One attempt at retro-deforming Zealandia using continuous and distributed deformation was made by Grobys et al. (2008). However, they restored only the crustal thickness of the New Caledonia Basin and Bounty Trough to the present day 24–20 km thickness of Zealandia's plateaus and rises. In this paper, we uniformly restore the crust of North Zealandia to a nominal pre-extension (pre-100 Ma) thickness of 35 km, that is, the same as present day eastern Australia (B. L. N. Kennett et al., 2011). Analogs for this unstretched crust would be a continental arc of moderate thickness such as the modern Aleutians or Patagonia. The crust may have been thicker or thinner in places and the 35 km value is just a typical value.

We use the deforming mesh workflow of Potter (2012) and Müller et al. (2018), in the GPlates plate rotation framework of Matthews et al. (2016). The results are shown in Figure 10. In this figure, the Marion and Challenger Plateaus have not been retrodeformed, so the Gondwana continent-ocean boundary oceanward of these places still has a bulge. A related feature not addressed in Figure 10 is the retrodeformation of the oroclinal bend as the Median Batholith approaches New Zealand from the north. However, the middle part of Figure 10 does show much of North Zealandia in a more correct pre-rift (unstretched) Cretaceous configuration than previous reconstructions. Restoration of the New Zealand oroclinal bend, the Marion Plateau and continental blocks around the Marion Plateau are outside the scope of this paper because appropriate constraints are currently lacking. However, Figure 10 does give an idea of the resulting "tight" paleogeography that could be achieved. Figure 10 also improves earlier maps (e.g., Gaina et al., 1998) in that it dispenses the need for hypothetical modeled faults between rigid blocks for which there is no geological evidence, such as Barcoo-Elizabeth-Fairway and Bellona-Aotea lineaments.

The reconstruction of Figure 10 serves to reaffirm that (a) what is now onland New Zealand was formerly spatially close to, and across geological strike from, Tasmania; (b) New Zealand was spatially distant, and along geological strike from, the east coast of mainland Australia; (c) the North Zealandia continental margin (a subduction zone in the Early Cretaceous) was essentially straight and trended north-south; and (d) the Mesozoic arc-trench gap (i.e., distance between the Median Batholith and continent-ocean boundary) was ~200 km that is, similar to the present day Taupo Volcanic Zone.

## 7. Conclusions

The R/V *Investigator* 2016T01 voyage to the Fairway Ridge obtained Late Cretaceous pebbly to cobbly sandstones, bedded sandstones, carbonaceous mudstones, and 41–36 Ma Eocene intraplate lavas including a nephelinite (Mortimer et al., 2019; this study). The plutonic and volcanic cobbles and pebbles in the sandstone were eroded from an Early Cretaceous magmatic arc which is presumed to still lie close to the Fairway Ridge. Previously only hydrothermally altered Late Cretaceous intraplate basalts had been obtained from the Fairway Ridge (Mortimer et al., 2018).

Our new Fairway Ridge age and composition data, along with a map of continental magnetic anomalies, enable extrapolation of high-level onland geological units from New Zealand and New Caledonia across all of North Zealandia. Positive magnetic anomalies help map the likely distribution of intraplate lavas across North Zealandia; some of these lavas are Late Cretaceous to Paleogene and relate to rifting and breakup of Zealandia from Gondwana. A pre-rift, Early Cretaceous tectonic reconstruction made using a deforming mesh model produces a tight fit of a long, thick, and narrow Zealandia against Australia.

The new basement geological map of North Zealandia in this paper (Figure 9) complements an earlier geological map of South Zealandia (Figure 12 of Tulloch et al. (2019)). Thus, the basement and sedimentary basin geological framework of the entire, ~5 Mkm$^2$, 95% submerged Zealandia continent has now been outlined in

reconnaissance. The submarine shelves of Earth's continents typically are mapped as separate, poorly characterized tectonic elements different from onland units (e.g., Hasterok et al., 2022). We believe Zealandia is the first of Earth's continents to have its basement, sedimentary basins and volcanic rocks fully mapped out to the continent-ocean boundary.

## Conflict of Interest

The authors declare they have no real or perceived financial conflicts of interest, or other affiliations that may be perceived as having conflicts of interest with respect to the results of this paper. Any use of trade, firm, or product names is for descriptive purposes only and does not imply endorsement by the U.S. Government.

## Data Availability Statement

Data used for this paper are available as eight Supplemental Files in Supporting Information S2, and on Figshare at https://doi.org/10.6084/m9.figshare.23348477.

Supplemental File 1. Analytical methods
Supplemental File 2. Zircon cathodoluminescence images
Supplemental File 3. Zircon data Otago 2018
Supplemental File 4. Zircon data UCSB
Supplemental File 5. Zircon data Otago 2022
Supplemental File 6. Zircon data MIT
Supplemental File 7. Zircon data Curtin and Heidelberg
Supplemental File 8. Ar-Ar data and plots USGS

**Acknowledgments**
We thank the crew of R/V *Investigator* voyage IN2016T01, especially Captain John Highton, and Australia's CSIRO Marine National Facility Voyage Managers Lisa Woodward and Doug Thost. Generous onboard help was given by our colleagues Jo Whittaker, Nick Herold, Lena O'Toole, Isabelle Sauermilch, Joanna Tobin, and Serena Yeung. We acknowledge the Parc Naturel de la Mer de Corail, Direction des Affaires Maritimes de la Nouvelle-Calédonie, and the Government of New Caledonia for authorizing rock dredging work on the Fairway Ridge. Permission to reproduce seismic line P702C was granted by Fugro NV. Post-voyage technical assistance was provided by Ben Durrant, John Simes, Belinda Smith Lyttle, Malcolm Reid, Noreen Evans, Brad McDonald, and Thomas Ludwig. Earlier versions of the manuscript were improved by comments from Nathan Daczko, Jim Calzia, Michael Clynne, Jacqueline Halpin, Jonathan Aitchison, and an anonymous reviewer. Mortimer's work was funded by New Zealand Ministry of Business, Innovation and Employment, Strategic Science Investment Fund Grant C05X1702 to GNS Science's *Understanding Te Riu-a Māui/Zealandia* Research Programme and by a New Zealand Government James Cook Research Fellowship, administered by the Royal Society Te Apārangi.

## References

Adams, C. J., Campbell, H. J., Mortimer, N., & Griffin, W. L. (2017). Perspectives on Cretaceous Gondwana break-up from detrital zircon provenance of southern Zealandia sandstones. *Geological Magazine*, *154*(4), 661–682. https://doi.org/10.1017/S0016756816000285

Adams, C. J., Mortimer, N., Campbell, H. J., & Griffin, W. L. (2015). Detrital zircon ages in Buller and Takaka terranes, New Zealand: Constraints on early Zealandia history. *New Zealand Journal of Geology and Geophysics*, *58*(2), 176–201. https://doi.org/10.1080/00288306.2015.1025798

Adams, C. J., Mortimer, N., Campbell, H. J., & Griffin, W. L. (2022). Detrital zircon provenance of Permian to Triassic Gondwana sequences, Zealandia and eastern Australia. *New Zealand Journal of Geology and Geophysics*, *65*(3), 457–469. https://doi.org/10.1080/00288306.2021.1954957

Arnot, M. J., & Bland, K. J. (2016). Atlas of petroleum prospectivity, Northwest Province: ArcGIS geodatabase and technical report. In *GNS Science data series 23b*. GNS Science.

Bache, F., Sutherland, R., Stagpoole, V., Herzer, R. H., Collot, J., & Rouillard, P. (2012). Stratigraphy of the southern Norfolk Ridge and the Reinga Basin: A record of initiation of Tonga–Kermadec–Northland subduction in the southwest Pacific. *Earth and Planetary Science Letters*, *321–322*, 41–53. https://doi.org/10.1016/j.epsl.2011.12.041

Borst, A. M., Waight, T. E., Finch, A. A., Storey, M., & Le Roux, P. J. (2018). Dating agpaitic rocks: A multi-system (U/Pb, Sm/Nd, Rb/Sr and $^{40}Ar/^{39}Ar$) isotopic study of layered nepheline syenites from the Ilímaussaq complex, Greenland. *Lithos*, *324–325*, 74–88. https://doi.org/10.1016/j.lithos.2018.10.037

Bryan, S. E., Ewart, A., Stephens, C. J., Parianos, J., & Downes, P. J. (2000). The Whitsunday volcanic province, central Queensland, Australia: Lithological and stratigraphic investigations of a silicic-dominated large igneous province. *Journal of Volcanology and Geothermal Research*, *99*(1–4), 55–78. https://doi.org/10.1016/S0377-0273(00)00157-8

Bryan, S. E., & Purdy, D. J. (2013). Whitsunday large silicic igneous province. In P. A. Jell (Ed.), *Geology of Queensland* (pp. 552–565). Queensland Department of Natural Resources and, Mines.

Calvert, A. T. (2023). Argon geochronology results for reconnaissance basement geology and tectonics of North Zealandia [Dataset]. USGS Data Release. Retrieved from https://www.sciencebase.gov/catalog/item/650090c3d34ed30c2057f6c6

Calvert, A. T., & Lanphere, M. A. (2006). Argon geochronology of Kilauea's early submarine history. *Journal of Volcanology and Geothermal Research*, *151*(1–3), 1–18. https://doi.org/10.1016/j.jvolgeores.2005.07.023

Campbell, M. J., Rosenbaum, G., Allen, C. M., & Spandler, C. (2020). Continental crustal growth processes revealed by detrital zircon petrochronology: Insights from Zealandia. *Journal of Geophysical Research: Solid Earth*, *125*(8), e2019JB019075. https://doi.org/10.1029/2019JB019075

Collot, J., Géli, L., Lafoy, Y., Vially, R., Cluzel, D., Klingelhoefer, F., & Nouzé, H. (2008). Tectonic history of northern New Caledonia basin from deep offshore seismic reflection: Relation to late Eocene obduction in New Caledonia, southwest Pacific. *Tectonics*, *27*(6), TC6006. https://doi.org/10.1029/2008TC002263

Collot, J., Herzer, R. H., Lafoy, Y., & Géli, L. (2009). Mesozoic history of the Fairway-Aotea basin: Implications for the early stages of Gondwana fragmentation. *Geochemistry, Geophysics, Geosystems*, *10*(12), Q12019. https://doi.org/10.1029/2009GC002612

Collot, J., Patriat, M., Etienne, S., Rouillard, P., Soetaert, F., Juan, C., et al. (2017). Deepwater fold-and-thrust belt along New Caledonia's western margin: Relation to post-obduction vertical motions. *Tectonics*, *36*(10), 2108–2122. https://doi.org/10.1002/2017TC004542

Collot, J., Patriat, M., Sutherland, R., Williams, S., Cluzel, D., Seton, M., et al. (2020). Geodynamics of the SW Pacific: A brief review and relations with New Caledonian geology. *Geological Society, London, Memoir*, *51*(1), 13–26. https://doi.org/10.1144/M51-2018-5

Collot, J., Sutherland, R., Etienne, S., Patriat, M., Roest, W. R., Marcaillou, B., et al. (2023). The Norfolk Ridge: A proximal record of the Tonga-Kermadec subduction initiation. *Geochemistry, Geophysics, Geosystems*, *24*(3), e2022GC010721. https://doi.org/10.1029/2022GC010721

Collot, J., Vendé-Leclerc, M., Rouillard, P., Lafoy, Y., & Géli, L. (2011). *Structural provinces of the southwest Pacific map*. Geological Survey of New Caledonia – DIMENC.

Cooper, R. A., & Tulloch, A. J. (1992). Early Palaeozoic terranes in New Zealand and their relationship to the Lachlan fold belt. *Tectonophysics*, *214*(1–4), 129–144. https://doi.org/10.1016/0040-1951(92)90193-A

Crawford, A. J. (2004). Voyage summary southern surveyor 01/2003. Unpublished CSIRO report. Retrieved from https://www.marine.csiro.au/data/reporting/get_file.cfm?eov_pub_id=866

Davy, B. W. (1991). Magnetic anomalies of the New Zealand basement. In *1991 New Zealand oil conference proceedings*: (pp. 134–144). Ministry of Commerce.

Ducea, M. N., Saleeby, J. B., & Bergantz, G. (2015). The architecture, chemistry, and evolution of continental magmatic arcs. *Annual Review of Earth and Planetary Sciences*, *43*(1), 299–331. https://doi.org/10.1146/annurev-earth-060614-105049

Etienne, S., Le Roy, P., Tournadour, E., Roest, W. R., Jorry, S., Collot, J., et al. (2021). Large-scale margin collapses along a partly drowned, isolated carbonate platform (Lansdowne Bank, SW Pacific Ocean). *Marine Geology*, *436*, 106477. https://doi.org/10.1016/j.margeo.2021.106477

Exon, N. F., Bernardel, G., Brown, J., Cortese, A., Findlay, C., Hoffmann, K., et al. (2006a). The geology of the Mellish Rise region off northeast Australia: A key piece in a tectonic puzzle – Southern surveyor cruise SS02/2005 – Geoscience Australia survey 274. Geoscience Australia Record, 2006/08.

Exon, N. F., Hill, P. J., Lafoy, Y., Heine, C., & Bernardel, G. (2006b). Kenn Plateau off northeast Australia: A continental fragment in the southwest Pacific jigsaw. *Australian Journal of Earth Sciences*, *53*(4), 541–564. https://doi.org/10.1080/08120090600632300

Farrington, R. J., Stegman, D. R., Moresi, L. N., Sandiford, M., & May, D. A. (2010). Interactions of 3D mantle flow and continental lithosphere near passive margins. *Tectonophysics*, *483*(1–2), 20–28. https://doi.org/10.1016/j.tecto.2009.10.008

Förster, H.-J., Tischendorf, G., & Trumbull, R. B. (1997). An evaluation of the Rb vs. (Y + Nb) discrimination diagram to infer tectonic setting of silicic igneous rocks. *Lithos*, *40*(2–4), 261–293. https://doi.org/10.1016/S0024-4937(97)00032-7

Frey, H. (1985). Magsat and POGO magnetic anomalies over the Lord Howe Rise: Evidence against a simple continental crustal structure. *Journal of Geophysical Research*, *90*(B3), 2631–2639. https://doi.org/10.1029/JB090iB03p02631

Gaina, C., Müller, R. D., Royer, J.-Y., Stock, J., Hardebeck, J., & Symonds, P. (1998). The tectonic history of the Tasman Sea: A puzzle with 13 pieces. *Journal of Geophysical Research*, *103*(B6), 12413–12433. https://doi.org/10.1029/98JB00386

Gaina, C., Müller, R. D., Royer, J.-Y., & Symonds, P. (1999). Evolution of the Louisiade triple junction. *Journal of Geophysical Research*, *104*(B6), 12927–12939. https://doi.org/10.1029/1999JB900038

Gallais, F., Fujie, G., Boston, B., Hackney, R., Kodaira, S., Miura, S., et al. (2019). Crustal structure across the Lord Howe Rise, northern Zealandia, and rifting of the eastern Gondwana margin. *Journal of Geophysical Research: Solid Earth*, *124*(3), 3036–3056. https://doi.org/10.1029/2018jb016798

Gans, P. B., Mortimer, N., Patriat, M., Turnbull, R. E., Crundwell, M. P., Agranier, A., et al. (2023). Detailed $^{40}Ar/^{39}Ar$ geochronology of the Loyalty and Three Kings Ridges clarifies the extent and sequential development of Eocene to Miocene southwest Pacific remnant volcanic arcs. *Geochemistry, Geophysics, Geosystems*, *24*(2), e2022GC010670. https://doi.org/10.1029/2022GC010670

Glen, R. A., & Cooper, R. A. (2021). Evolution of the east Gondwana convergent margin in Antarctica, southern Australia and New Zealand from the Neoproterozoic to latest Devonian. *Earth-Science Reviews*, *220*, 103687. https://doi.org/10.1016/j.earscirev.2021.103687

Griffiths, J. R. (1971). Reconstruction of the south-west Pacific margin of Gondwanaland. *Nature*, *234*(5326), 203–207. https://doi.org/10.1038/234203a0

Grindley, G. W., & Davey, F. J. (1982). The reconstruction of New Zealand, Australia, and Antarctica. In C. Craddock (Ed.), *Antarctic Geoscience* (pp. 15–29). University of Wisconsin Press.

Grobys, J. W. G., Gohl, K., & Eagles, G. (2008). Quantitative tectonic reconstructions of Zealandia based on crustal thickness estimates. *Geochemistry, Geophysics, Geosystems*, *9*(1), Q01005. https://doi.org/10.1029/2007GC001691

Grobys, J. W. G., Gohl, K., Uenzelmann-Neben, G., Davy, B., & Barker, D. (2009). Extensional and magmatic nature of the Campbell Plateau and great south basin from deep crustal studies. *Tectonophysics*, *472*(1–4), 213–225. https://doi.org/10.1016/j.tecto.2008.05.003

Hasterok, D., Halpin, J. A., Collins, A. S., Hand, M., Kreemer, C., Gard, M. G., & Glorie, S. (2022). New maps of global geological provinces and tectonic plates. *Earth-Science Reviews*, *231*, 104069. https://doi.org/10.1016/j.earscirev.2022.104069

Henderson, R., Spandler, C., Foley, E. K., Kemp, A. I. S., Roberts, E. M., & Fisher, C. (2022). Early Cretaceous tectonic setting of eastern Australia: Evidence from the subduction-related Morton igneous association of southeast Queensland. *Lithos*, *410–411*, 106573. https://doi.org/10.1016/j.lithos.2021.106573

Herzer, R. H., Davy, B. W., Mortimer, N., Quilty, P. G., Chaproniere, G. C. H., Jones, C. M., et al. (2009). Seismic stratigraphy and structure of the Northland Plateau and the development of the Vening Meinesz transform margin, SW Pacific Ocean. *Marine Geophysical Researches*, *30*(1), 21–60. https://doi.org/10.1007/s11001-009-9065-1

Higgins, K., Hashimoto, T., Rollet, N., Colwell, J., Hackney, R., & Milligan, P. (2015). Structural analysis of extended Australian continental crust: Capel and Faust basins, Lord Howe Rise. *Geological Society, London, Special Publication*, *413*(1), 9–33. https://doi.org/10.1144/SP413.6

Ireland, T. R., & Gibson, G. M. (1998). SHRIMP monazite and zircon geochronology of high-grade metamorphism in New Zealand. *Journal of Metamorphic Geology*, *16*(2), 149–167. https://doi.org/10.1111/j.1525-1314.1998.00112.x

Isaac, M. J., Herzer, R. H., Brook, F. J., & Hayward, B. W. (1994). *Cretaceous and Cenozoic sedimentary basins of Northland, New Zealand* (Vol. 8). Institute of Geological & Nuclear Sciences Monograph.

Karthikeyan, V., Collot, J., Etienne, S., Loubrieu, B., Patriat, M., Vendé-Leclerc, M., et al. (2022). Base de données de sondeurs multifaisceaux et modèles bathymétriques de la Nouvelle-Calédonie-hors lagon. *Rapport SGNC*, *2022*(12). https://doi.org/10.13155/91834

Kennett, B. L. N., Salmon, M., Saygin, E., & Group, A. W. (2011). AusMoho: The variation of Moho depth in Australia. *Geophysical Journal International*, *187*(2), 946–958. https://doi.org/10.1111/j.1365-246X.2011.05194.x

Kennett, J., von der Borch, C. C., Baker, P. A., Barton, C. E., Boersma, A., Caulet, J. P., et al. (1986). Site 587: Lansdowne bank, southwest Pacific. *Initial Reports of the Deep Sea Drilling Project*, *90*, 115–138. https://doi.org/10.2973/dsdp.proc.90.103.1986

Klingelhoefer, F., Lafoy, Y., Collot, J., Cosquer, E., Géli, L., Nouzé, H., & Vially, R. (2007). Crustal structure of the basin and ridge system west of New Caledonia (southwest Pacific) from wide-angle and reflection seismic data. *Journal of Geophysical Research*, *112*(B11), B11102. https://doi.org/10.1029/2007JB005093

Korsch, R. J., Adams, C. J., Black, L. P., Foster, D. A., Fraser, G. L., Murray, C. G., et al. (2009). Geochronology and provenance of the late Paleozoic accretionary wedge and Gympie terrane, new England Orogen, eastern Australia. *Australian Journal of Earth Sciences*, *56*(5), 655–685. https://doi.org/10.1080/08120090902825776

Lafoy, Y., Brodien, I., Vially, R., & Exon, N. F. (2005). Structure of the basin and ridge system west of New Caledonia (southwest Pacific): A synthesis. *Marine Geophysical Researches*, *26*(1), 37–50. https://doi.org/10.1007/s11001-005-5184-5

Lapouille, A. (1977). Magnetic surveys over the rises and basins in the south-west Pacific. In *International Symposium on Geodynamics in South-West Pacific, Nouméa (New Caledonia), 1976* (pp. 15–28). Editions Technip.
Le Maitre, R. W. (1989). *A classification of igneous rocks and glossary of terms*. Blackwell Scientific.
Ludwig, K. (2008). *Isoplot 4.13; A geochronological toolkit for Microsoft excel* (Vol. 4). Berkeley Geochronology Centre Special Publication.
Matthews, K. J., Maloney, K. T., Zahirovic, S., Williams, S. E., Seton, M., & Müller, R. D. (2016). Global plate boundary evolution and kinematics since the late Paleozoic. *Global and Planetary Change*, *146*, 226–250. https://doi.org/10.1016/j.gloplacha.2016.10.002
Maurizot, P., Cluzel, D., Meffre, S., Campbell, H. J., Collot, J., & Sevin, B. (2020a). Pre-Late Cretaceous basement terranes of the Gondwana active margin. *Geological Society, London, Memoir*, *51*(1), 27–52. https://doi.org/10.1144/M51-2016-11
Maurizot, P., Cluzel, D., Patriat, M., Collot, J., Iseppi, M., Lesimple, S., et al. (2020b). The Eocene subduction-obduction complex of New Caledonia. *Geological Society, London, Memoir*, *51*(1), 93–130. https://doi.org/10.1144/M51-2018-70
McDougall, I., Maboko, M. A. H., Symonds, P. A., McCulloch, M. T., Williams, I. S., & Kudrass, H. R. (1994). Dampier Ridge, Tasman Sea, as a stranded continental fragment. *Australian Journal of Earth Sciences*, *41*(5), 395–406. https://doi.org/10.1080/08120099408728150
Meffre, S., Crawford, A. J., & Quilty, P. G. (2006). Arc-continent collision forming a large island between New Caledonia and New Zealand in the Oligocene. *ASEG Extended Abstracts*, *2006*(1), 1–3. https://doi.org/10.1071/ASEG2006ab111
Meyer, B., Saltus, R., & Chulliat, A. (2017). *EMAG2: Earth magnetic anomaly grid (2-arc-minute resolution) version 3*. National Centers for Environmental Information, NOAA, National Oceanic and Atmospheric Administration. https://doi.org/10.7289/V5H70CVX
Mignot, A. (1984). *Sismo-stratigraphie de la terminaison nord de la ride de Lord Howe. Evolution géodynamique du Sud-Ouest Pacifique entre l'Australie et la Nouvelle-Calédonie*. Unpublished PhD thesis, Université Pierre et Marie Curie.
Mortimer, N. (2004). Basement gabbro from the Lord Howe Rise. *New Zealand Journal of Geology and Geophysics*, *47*(3), 501–507. https://doi.org/10.1080/00288306.2004.9515072
Mortimer, N., Adams, C. J., & Wright, I. C. (2020). Early Cretaceous greywacke from Colville Knolls, New Zealand. *New Zealand Journal of Geology and Geophysics*, *63*(1), 145–150. https://doi.org/10.1080/00288306.2019.1629967
Mortimer, N., Campbell, H. J., Tulloch, A. J., King, P. R., Stagpoole, V. M., Wood, R. A., et al. (2017). Zealandia: Earth's hidden continent. *Geological Society of America Today*, *27*(3), 28–35. https://doi.org/10.1130/GSATG321A.1
Mortimer, N., Dadd, K. A., O'Toole, L., Crundwell, M., Seton, M., Williams, S. E., et al. (2019). Eocene nephelinite and basanite from the Fairway Ridge, North Zealandia. *Deep-Sea Research Part I*, *152*, 103101. https://doi.org/10.1016/j.dsr.2019.103101
Mortimer, N., Gans, P. B., Meffre, S., Martin, C. E., Seton, M., Williams, S. E., et al. (2018). Regional volcanism of northern Zealandia: Post-Gondwana break-up magmatism on an extended, submerged continent. *Geological Society, London, Special Publication*, *463*(1), 199–226. https://doi.org/10.1144/SP463.9
Mortimer, N., Gans, P. B., Palin, J. M., Herzer, R. H., Pelletier, B., & Monzier, M. (2014a). Eocene and Oligocene basins and ridges of the Coral Sea-New Caledonia region: Tectonic link between Melanesia, Fiji, and Zealandia. *Tectonics*, *33*(7), 1386–1407. https://doi.org/10.1002/2014TC003598
Mortimer, N., Gans, P. B., Palin, J. M., Meffre, S., Herzer, R. H., & Skinner, D. N. B. (2010). Location and migration of Miocene–Quaternary volcanic arcs in the SW Pacific region. *Journal of Volcanology and Geothermal Research*, *190*(1–2), 1–10. https://doi.org/10.1016/j.jvolgeores.2009.02.017
Mortimer, N., Hauff, F., & Calvert, A. T. (2008). Continuation of the new England Orogen, Australia, beneath the Queensland Plateau and Lord Howe Rise. *Australian Journal of Earth Sciences*, *55*(2), 195–209. https://doi.org/10.1080/08120090701689365
Mortimer, N., Herzer, R. H., Gans, P. B., Parkinson, D. L., & Seward, D. (1998). Basement geology from three Kings Ridge to West Norfolk Ridge, southwest Pacific Ocean: Evidence from petrology, geochemistry and isotopic dating of dredge samples. *Marine Geology*, *148*(3–4), 135–162. https://doi.org/10.1016/S0025-3227(98)00007-3
Mortimer, N., Patriat, M., Gans, P. B., Agranier, A., Chazot, G., Collot, J., et al. (2021). The Norfolk Ridge seamounts: Eocene–Miocene volcanoes near Zealandia's rifted continental margin. *Australian Journal of Earth Sciences*, *68*(3), 368–380. https://doi.org/10.1080/08120099.2020.1805007
Mortimer, N., Raine, J. I., & Cook, R. A. (2009). Correlation of basement rocks from Waka Nui-1 and Awhitu-1, and the Jurassic regional geology of Zealandia. *New Zealand Journal of Geology and Geophysics*, *52*, 1–10. https://doi.org/10.1080/00288300909509873
Mortimer, N., Rattenbury, M. S., King, P. R., Bland, K. J., Barrell, D. J. A., Bache, F., et al. (2014b). High-level stratigraphic scheme for New Zealand rocks. *New Zealand Journal of Geology and Geophysics*, *57*(4), 402–419. https://doi.org/10.1080/00288306.2014.946062
Mortimer, N., & Scott, J. M. (2020). Volcanoes of Zealandia and the southwest Pacific. *New Zealand Journal of Geology and Geophysics*, *63*(4), 371–377. https://doi.org/10.1080/00288306.2020.1713824
Mortimer, N., Smith Lyttle, B., & Black, J. (2020). *Tectonic map of Te Riu-a-Māui/Zealandia. Scale 1:8 500 000*. GNS Science Poster, 8. https://doi.org/10.21420/M90C-5J03
Mortimer, N., Tulloch, A. J., & Ireland, T. R. (1997). Basement geology of Taranaki and Wanganui basins, New Zealand. *New Zealand Journal of Geology and Geophysics*, *40*(2), 223–236. https://doi.org/10.1080/00288306.1997.9514754
Mortimer, N., Tulloch, A. J., Spark, R. N., Walker, N. W., Ladley, E., Allibone, A., & Kimbrough, D. (1999). Overview of the Median Batholith, New Zealand: A new interpretation of the geology of the Median Tectonic Zone. *Journal of African Earth Sciences*, *29*(1), 257–268. https://doi.org/10.1016/S0899-5362(99)00095-0
Mortimer, N., Turnbull, R. E., Palin, J. M., Tulloch, A. J., Rollet, N., & Hashimoto, T. (2015). Triassic–Jurassic granites on the Lord Howe Rise, northern Zealandia. *Australian Journal of Earth Sciences*, *62*, 735–742. https://doi.org/10.1080/08120099.2015.1081984
Mortimer, N., Williams, S. E., Seton, M., Calvert, A. T., Waight, T. E., Turnbull, R. E., et al. (2023). Reconnaissance basement geology and tectonics of North Zealandia. Supplemental Files 1-8 [Dataset]. Figshare. https://doi.org/10.6084/m9.figshare.23348477
Muir, R. J., Ireland, T. R., Weaver, S. D., Bradshaw, J. D., Evans, J. A., Eby, G. N., & Shelley, D. (1998). Geochronology and geochemistry of a Mesozoic magmatic arc system, Fiordland, New Zealand. *Journal of the Geological Society, London*, *155*(6), 1037–1053. https://doi.org/10.1144/gsjgs.155.6.1037
Muir, R. J., Weaver, S. D., Bradshaw, J. D., Eby, G. N., & Evans, J. A. (1995). The Cretaceous separation point batholith, New Zealand: Granitoid magmas formed by partial melting of mafic lithosphere. *Journal of the Geological Society, London*, *152*(4), 689–701. https://doi.org/10.1144/gsjgs.152.4.0689
Müller, R. D., Russell, S. H. J., Zahirovic, S., Williams, S. E., & Williams, C. S. (2018). Modelling and visualising distributed crustal deformation of Australia and Zealandia using GPlates 2.0. *ASEG Extended Abstracts*, *2018*(1), 1–7. https://doi.org/10.1071/ASEG2018abT6_2A
Nebel, O., Münker, C., Nebel-Jacobsen, Y. J., Kleine, T., Mezger, T., & Mortimer, N. (2007). Hf–Nd–Pb isotope evidence from Permian arc rocks for the long-term presence of the Indian–Pacific mantle boundary in the SW Pacific. *Earth and Planetary Science Letters*, *254*(3–4), 377–392. https://doi.org/10.1016/j.epsl.2006.11.046

Nelson, D. A., & Cottle, J. M. (2017). Long-term geochemical and geodynamic segmentation of the paleo-Pacific margin of Gondwana: Insight from the Antarctic and adjacent sectors. *Tectonics*, *36*(12), 3229–3247. https://doi.org/10.1002/2017TC004611

Norvick, M. S., Langford, R. P., Hashimoto, T., Rollet, N., Higgins, K. L., & Morse, M. P. (2008). New insights into the evolution of the Lord Howe Rise (Capel and Faust basins), offshore eastern Australia, from terrane and geophysical data analysis. In *PESA Eastern Australasian Basins Symposium, III* (pp. 291–309).

Orr, D., Sutherland, R., & Stratford, W. R. (2020). Eocene to Miocene subduction initiation recorded in stratigraphy of Reinga Basin, northwest New Zealand. *Tectonics*, *39*(2), e2019TC005899. https://doi.org/10.1029/2019TC005899

Patriat, M., Collot, J., Etienne, S., Poli, S., Clerc, C., Mortimer, N., et al. (2018). New Caledonia obducted peridotite Nappe: Offshore extent and implications for obduction and post-obduction processes. *Tectonics*, *37*(4), 1077–1096. https://doi.org/10.1002/2017TC004722

Pattier, F., Etienne, S., Collot, J., Patriat, M., Tournadour, E., Roest, W. R., & Rouillard, P. (2019). Neogene-Quaternary architecture and sedimentary processes on an isolated carbonate-fed deep-water basin (Fairway Basin, Southwest Pacific). *Marine Geology*, *413*, 27–47. https://doi.org/10.1016/j.margeo.2019.04.003

Pearce, J. A. (1996). A users guide to basalt discrimination diagrams. In D. A. Wyman (Ed.), *Trace element geochemistry of volcanic rocks: Applications for massive sulphide exploration* (Vol. 12, pp. 79–113). Geological Association of Canada Short Course Notes.

Pearce, J. A., Harris, N. B. W., & Tindle, A. G. (1984). Trace element discrimination diagrams for the tectonic interpretation of granitic rocks. *Journal of Petrology*, *25*(4), 956–983. https://doi.org/10.1093/petrology/25.4.956

Potter, J. M. (2012). *Modelling the history of extension and subduction east of Australia*. Unpublished BSc (Hons) thesis, University of Sydney.

Price, R. C., Spandler, C., Arculus, R., & Reay, A. E. (2011). The Longwood igneous complex, Southland, New Zealand: A Permo-Jurassic, intra-oceanic, subduction-related, I-type batholithic complex. *Lithos*, *126*(1–2), 1–21. https://doi.org/10.1016/j.lithos.2011.04.006

Ramezani, J., Beveridge, T. L., Rogers, R. R., Eberth, D. A., & Roberts, E. M. (2022). Calibrating the zenith of dinosaur diversity in the Campanian of the western interior basin by CA-ID-TIMS U–Pb geochronology. *Scientific Reports*, *12*(1), 16026. https://doi.org/10.1038/s41598-022-19896-w

Ravenne, C., de Broin, C. E., Dupont, J. P., Lapouille, A., & Launay, J. (1977). New Caledonia basin-Fairway ridge: Structural and sedimentary study. In *International Symposium on Geodynamics in South-West Pacific, Nouméa (New Caledonia)* (Vol. 1976, pp. 145–154). Editions Technip.

Riefstahl, F., Gohl, K., Davy, B., Hoernle, K., Mortimer, N., Timm, C., et al. (2020). Cretaceous intracontinental rifting at the southern Chatham Rise margin and initialisation of seafloor spreading between Zealandia and Antarctica. *Tectonophysics*, *776*, 228298. https://doi.org/10.1016/j.tecto.2019.228298

Ringwood, M. F., Schwartz, J. J., Turnbull, R. E., & Tulloch, A. J. (2021). Phanerozoic record of mantle-dominated arc magmatic surges in the Zealandia Cordillera. *Geology*, *49*(10), 1230–1234. https://doi.org/10.1130/G48916.1

Rogers, A., Flanigan, M., Nebel, O., Nebel-Jacobsen, Y., Wang, X., Arculus, R. J., et al. (2023). The isotopic origin of Lord Howe Island reveals secondary mantle plume twinning in the Tasman Sea. *Chemical Geology*, *622*, 121374. https://doi.org/10.1016/j.chemgeo.2023.121374

Rosenbaum, G. (2018). The Tasmanides: Phanerozoic tectonic evolution of eastern Australia. *Annual Review of Earth and Planetary Sciences*, *46*(1), 291–325. https://doi.org/10.1146/annurev-earth-082517-010146

Roser, B. P., & Korsch, R. J. (1986). Determination of tectonic setting of sandstone-mudstone suites using $SiO_2$ content and $K_2O/Na_2O$ ratio. *The Journal of Geology*, *94*(5), 635–650. https://doi.org/10.1086/629071

Rouillard, P., Collot, J., Sutherland, R., Bache, F., Patriat, M., Etienne, S., & Maurizot, P. (2017). Seismic stratigraphy and paleogeographic evolution of Fairway Basin, northern Zealandia, southwest Pacific: From Cretaceous Gondwana breakup to Cenozoic Tonga–Kermadec subduction. *Basin Research*, *29*, 189–212. https://doi.org/10.1111/bre.12144

Sagar, M. W., Palin, J. M., Tulloch, A. J., & Heath, L. A. (2016). The geology, geochronology and affiliation of the Glenroy Complex and adjacent plutonic rocks, southeast Nelson. *New Zealand Journal of Geology and Geophysics*, *59*(2), 213–235. https://doi.org/10.1080/00288306.2015.1101004

Schreckenberger, B., Roeser, W. A., & Symonds, P. A. (1992). Marine magnetic anomalies over the Lord Howe Rise and the Tasman Sea: Implications for the magnetization of the lower continental crust. *Tectonophysics*, *212*(1–2), 77–97. https://doi.org/10.1016/0040-1951(92)90141-R

Schwartz, J. J., Andico, S., Turnbull, R. E., Klepeis, K. A., Tulloch, A. J., Kitajima, K., & Valley, J. W. (2021). Stable and transient isotopic trends in the crustal evolution of Zealandia Cordillera. *American Mineralogist*, *106*(9), 1369–1387. https://doi.org/10.2138/am-2021-7626

Seton, M., Mortimer, N., Williams, S. E., Quilty, P., Gans, P. B., Meffre, S., et al. (2016). Melanesian back-arc basin and arc development: Constraints from the eastern Coral Sea. *Gondwana Research*, *39*, 77–95. https://doi.org/10.1016/j.gr.2016.06.011

Seton, M., Williams, S. E., Mortimer, N., Meffre, S., Micklethwaite, S., & Zahirovic, S. (2019). Magma production along the Lord Howe seamount chain, northern Zealandia. *Geological Magazine*, *156*(9), 1605–1617. https://doi.org/10.1017/S0016756818000912

Shaanan, U., Rosenbaum, G., & Sihombing, F. M. H. (2018). Continuation of the Ross–Delamerian Orogen: Insights from eastern Australian detrital-zircon data. *Australian Journal of Earth Sciences*, *65*(7–8), 1123–1131. https://doi.org/10.1080/08120099.2017.1354916

Smith, W. H. F., & Sandwell, D. T. (1997). Global Sea floor topography from satellite altimetry and Ship depth Soundings. *Science*, *277*(5334), 1956–1962. https://doi.org/10.1126/science.277.5334.1956

Stagg, H. M. J., Borissova, I., Alcock, M., & Moore, A. M. G. (1999). Tectonic provinces of the Lord Howe Rise 'Law of the Sea' study has implications for Frontier hydrocarbons. *AGSO Research Newsletter*, *31*, 31–32.

Strogen, D. P., Seebeck, H., Hines, B. R., Bland, K. J., & Crampton, J. C. (2022). Palaeogeographic evolution of Zealandia: Mid-cretaceous to present. *New Zealand Journal of Geology and Geophysics*, *66*(3), 528–557. https://doi.org/10.1080/00288306.2022.2115520

Strong, D. T., Turnbull, R. E., Haubrock, S. N., & Mortimer, N. (2016). Petlab: New Zealand's national rock catalogue and geoanalytical database. *New Zealand Journal of Geology and Geophysics*, *59*(3), 475–481. https://doi.org/10.1080/00288306.2016.1157086

Sun, S. S., & McDonough, W. F. (1989). Chemical and isotopic systematics of oceanic basalts: Implications for mantle compositions and processes. *Geological Society, London, Special Publication*, *42*(1), 313–345. https://doi.org/10.1144/GSL.SP.1989.042.01.19

Sutherland, R. (1999). Basement geology and tectonic development of the greater New Zealand region: An interpretation from regional magnetic data. *Tectonophysics*, *308*(3), 341–362. https://doi.org/10.1016/S0040-1951(99)00108-0

Sutherland, R., Dickens, G. R., Blum, P., Agnini, C., Alegret, L., Asatryan, G., et al. (2020). Continental-scale geographic change across Zealandia during Paleogene subduction initiation. *Geology*, *48*(5), 419–424. https://doi.org/10.1130/G47008.1

Sutherland, R., Viskovic, G. P. D., Bache, F., Stagpoole, V. M., Collot, J., Rouillard, P., et al. (2012). Compilation of seismic reflection data from the Tasman Frontier region, southwest Pacific. GNS Science Report, 2012/01, (72 p.).

Timm, C., Hoernle, K., Werner, R., Hauff, F., van den Bogaard, P., White, J., et al. (2010). Temporal and geochemical evolution of the Cenozoic intraplate volcanism of Zealandia. *Earth-Science Reviews*, *98*(1–2), 38–64. https://doi.org/10.1016/j.earscirev.2009.10.002

Tulloch, A. J., Kimbrough, D. L., & Wood, R. A. (1991). Carboniferous granite basement dredged from a site on the southwest margin of the Challenger Plateau, Tasman Sea. *New Zealand Journal of Geology and Geophysics*, *34*(2), 121–126. https://doi.org/10.1080/00288306.1991.9514449

Tulloch, A. J., Mortimer, N., Ireland, T. R., Waight, T. E., Maas, R., Palin, J. M., et al. (2019). Reconnaissance basement geology and tectonics of South Zealandia. *Tectonics*, *38*(2), 516–551. https://doi.org/10.1029/2018TC005116

Turnbull, R. E., Schwartz, J. J., Fiorentini, M. L., Jongens, R., Evans, N. J., Ludwig, T., et al. (2021). A hidden Rodinian lithospheric keel beneath Zealandia, Earth's newly recognized continent. *Geology*, *49*, 1009–1014. https://doi.org/10.1130/G48711.1

Turnbull, R. E., Schwartz, J. J., Fiorentini, M. L., Klepeis, K. A., Jongens, R., Miranda, E., et al. (2023). Mapping the 4D lithospheric architecture of Zealandia using zircon O and Hf isotopes in plutonic rocks. *Gondwana Research*, *121*, 436–471. https://doi.org/10.1016/j.gr.2023.05.010

Turnbull, R. E., Tulloch, A. J., Ramezani, J., & Jongens, R. (2016). Extension-facilitated pulsed S-I-A-type "flare-up" magmatism at 370 Ma along the southeast Gondwana margin in New Zealand: Insights from U-Pb geochronology and geochemistry. *Geological Society of America Bulletin*, *128*(9–10), 1500–1520. https://doi.org/10.1130/B31426.1

Uruski, C. I. (2020). Seismic recognition of igneous rocks of the Deepwater Taranaki Basin, New Zealand, and their distribution. *New Zealand Journal of Geology and Geophysics*, *63*(2), 190–209. https://doi.org/10.1080/00288306.2019.1647253

Uruski, C. I. (2023). A possible Jurassic age for the New Caledonia Trough and implications for Zealandia's history. *New Zealand Journal of Geology and Geophysics*, 1–23. https://doi.org/10.1080/00288306.2023.2232584

van der Meer, Q. H. A., Waight, T. E., Tulloch, A. J., Whitehouse, M. J., & Andersen, T. (2018). Magmatic evolution during the Cretaceous transition from subduction to continental break-up of the eastern Gondwana margin (New Zealand) documented by in-situ zircon O–Hf isotopes and bulk-rock Sr–Nd isotopes. *Journal of Petrology*, *59*(5), 849–880. https://doi.org/10.1093/petrology/egy047

Veevers, J. J. (2012). Reconstructions before rifting and drifting reveal the geological connections between Antarctica and its conjugates in Gondwanaland. *Earth-Science Reviews*, *111*(3–4), 249–318. https://doi.org/10.1016/j.earscirev.2011.11.009

Williams, S. E., Mortimer, N., Etienne, S., Whittaker, J., Herold, N., O'Toole, L., et al. (2016). Voyage report for IN2016T01 eastern Coral Sea tectonics followup (ECOSAT II), R/V *Investigator*, June–July 2016. GNS Science Report, 2016/50 (56 p.).

## References From the Supporting Information

Black, L. P., Kamo, S. L., Allen, C. M., Davis, D. W., Aleinikoff, J. N., Valley, J. W., et al. (2004). Improved $^{206}Pb/^{238}U$ microprobe geochronology by the monitoring of a trace-element-related matrix effect; SHRIMP, ID-TIMS, ELA-ICP-MS and oxygen isotope documentation for a series of zircon standards. *Chemical Geology*, *205*(1–2), 115–140. https://doi.org/10.1016/j.chemgeo.2004.01.003

Blichert-Toft, J. (2008). The Hf isotopic composition of zircon reference material 91500. *Chemical Geology*, *253*(3–4), 252–257. https://doi.org/10.1016/j.chemgeo.2008.05.014

Bowring, J. F., McLean, N. M., & Bowring, S. A. (2011). Engineering cyber infrastructure for U-Pb geochronology: Tripoli and U-Pb_Redux. *Geochemistry, Geophysics, Geosystems*, *12*(6), Q0AA19. https://doi.org/10.1029/2010GC003479

Chu, N.-C., Taylor, R. N., Chavagnac, V., Nesbitt, R. W., Boella, R. M., Milton, J. A., et al. (2002). Hf isotope ratio analysis using multi-collector inductively coupled plasma mass spectrometry: An evaluation of isobaric interference corrections. *Journal of Analytical Atomic Spectrometry*, *17*(12), 1567–1574. https://doi.org/10.1039/b206707b

Condon, D. J., Schoene, B., McLean, N. M., Bowring, S. A., & Parrish, R. R. (2015). Metrology and traceability of U-Pb isotope dilution geochronology (EARTHTIME Tracer Calibration Part I). *Geochimica et Cosmochimica Acta*, *164*, 464–480. https://doi.org/10.1016/j.gca.2015.05.026

Cowan, G. A., & Adler, H. H. (1976). The variability of the natural abundance of $^{235}U$. *Geochimica et Cosmochimica Acta*, *40*(12), 1487–1490. https://doi.org/10.1016/0016-7037(76)90087-9

Fisher, C. M., Hanchar, J. M., Samson, S. D., Dhuime, B., Blichert-Toft, J., Vervoort, J. D., & Lam, R. (2011). Synthetic zircon doped with hafnium and rare earth elements: A reference material for in situ hafnium isotope analysis. *Chemical Geology*, *286*(1–2), 32–47. https://doi.org/10.1016/j.chemgeo.2011.04.013

Fleck, R. J., Hagstrum, J. T., Calvert, A. T., Evarts, R. C., & Conrey, R. M. (2014). $^{40}Ar/^{39}Ar$ geochronology, paleomagnetism, and evolution of the boring volcanic field, Oregon and Washington, USA. *Geosphere*, *10*(6), 1283–1314. https://doi.org/10.1130/GES00985.1

Hagen-Peter, G., Cottle, J. M., Tulloch, A. J., & Cox, S. C. (2015). Mixing between enriched lithospheric mantle and crustal components in a short-lived subduction-related magma system, Dry Valleys area, Antarctica: Insights from U-Pb geochronology, Hf isotopes, and whole-rock geochemistry. *Lithosphere*, *7*(2), 174–188. https://doi.org/10.1130/L384.1

Jackson, S. E., Pearson, N. J., Griffin, W. L., & Belousova, E. A. (2004). The application of laser ablation-inductively coupled plasma-mass spectrometry to in situ U–Pb zircon geochronology. *Chemical Geology*, *211*(1–2), 47–69. https://doi.org/10.1016/j.chemgeo.2004.06.017

Jaffey, A. H., Flynn, K. F., Glendenin, L. E., Bentley, W. C., & Essling, A. M. (1971). Precision measurement of half-lives and specific activities of $^{235}U$ and $^{238}U$. *Physical Review C*, *4*(5), 1889–1906. https://doi.org/10.1103/PhysRevC.4.1889

Jochum, K. P., Weis, U., Stoll, B., Kuzmin, D., Yang, Q., Raczek, I., et al. (2011). Determination of reference values for NIST SRM 610–617 glasses following ISO guidelines. *Geostandards and Geoanalytical Research*, *35*(4), 397–429. https://doi.org/10.1111/j.1751-908X.2011.00120.x

Kylander-Clark, A. R. C., Hacker, B. R., & Cottle, J. M. (2013). Laser-ablation split-stream ICP petrochronology. *Chemical Geology*, *345*, 99–112. https://doi.org/10.1016/j.chemgeo.2013.02.019

Liu, Y., Hu, Z., Zong, K., Gao, C., Gao, S., Xu, J., & Chen, H. (2010). Reappraisement and refinement of zircon U-Pb isotope and trace element analyses by LA-ICP-MS. *Chinese Science Bulletin*, *55*(15), 1535–1546. https://doi.org/10.1007/s11434-010-3052-4

Mattinson, J. M. (2005). Zircon U-Pb chemical abrasion ("CA-TIMS") method: Combined annealing and multi-step partial dissolution analysis for improved precision and accuracy of zircon ages. *Chemical Geology*, *220*(1–2), 47–66. https://doi.org/10.1016/j.chemgeo.2005.03.011

McLean, N. M., Bowring, J. F., & Bowring, S. A. (2011). An algorithm for U-Pb isotope dilution data reduction and uncertainty propagation. *Geochemistry, Geophysics, Geosystems*, *12*(6), Q0AA18. https://doi.org/10.1029/2010GC003478

McLean, N. M., Condon, D. J., Schoene, B., & Bowring, S. A. (2015). Evaluating uncertainties in the calibration of isotopic reference materials and multi-element isotopic tracers (EARTHTIME Tracer Calibration Part II). *Geochimica et Cosmochimica Acta*, *164*, 481–501. https://doi.org/10.1016/j.gca.2015.02.040

Patchett, P. J., & Tatsumoto, M. (1980). Hafnium isotope variations in oceanic basalts. *Geophysical Research Letters*, *7*(12), 1077–1080. https://doi.org/10.1029/GL007i012p01077

Patchett, P. J., & Tatsumoto, M. (1981). A routine high-precision method for Lu-Hf isotope geochemistry and chronology. *Contributions to Mineralogy and Petrology*, *75*(3), 263–267. https://doi.org/10.1007/BF01166766

Paton, C., Hellstrom, J., Paul, B., Woodhead, J., & Hergt, J. (2011). Iolite: Freeware for the visualisation and processing of mass spectrometric data. *Journal of Analytical Atomic Spectrometry*, *26*(12), 2508–2518. https://doi.org/10.1039/C1JA10172B

Paton, C., Woodhead, J. D., Hellstrom, J. C., Hergt, J. M., Greig, A., & Maas, R. (2010). Improved laser ablation U-Pb zircon geochronology through robust downhole fractionation correction. *Geochemistry, Geophysics, Geosystems*, *11*(3), Q0AA06. https://doi.org/10.1029/2009GC002618

Sambridge, M. S., & Compston, W. (1994). Mixture modeling of multi-component data sets with application to ion-probe zircon ages. *Earth and Planetary Science Letters*, *128*(3–4), 373–390. https://doi.org/10.1016/0012-821X(94)90157-0

Sláma, J., Košler, J., Condon, D. J., Crowley, J. L., Gerdes, A., Hanchar, J. M., et al. (2008). Plešovice zircon — A new natural reference material for U–Pb and Hf isotopic microanalysis. *Chemical Geology*, *249*(1–2), 1–35. https://doi.org/10.1016/j.chemgeo.2007.11.005

Spell, T. L., & McDougall, I. (2003). Characterization and calibration of $^{40}Ar/^{39}Ar$ dating standards. *Chemical Geology*, *198*(3–4), 189–211. https://doi.org/10.1016/S0009-2541(03)00005-6

Spencer, C. J., Cavosie, A. J., Raub, T. D., Rollinson, H., Jeon, H., Searle, M. P., et al. (2017). Evidence for melting mud in Earth's mantle from extreme oxygen isotope signatures in zircon. *Geology*, *45*(11), 975–978. https://doi.org/10.1130/G39402.1

Stacey, J. S., & Kramers, J. D. (1975). Approximation of terrestrial lead isotope evolution by a two-stage model. *Earth and Planetary Science Letters*, *26*(2), 207–221. https://doi.org/10.1016/0012-821X(75)90088-6

Steiger, R. H., & Jäger, E. (1977). Subcommission on geochronology: Convention on the use of decay constants in geo- and cosmochronology. *Earth and Planetary Science Letters*, *3*, 359–362. https://doi.org/10.1016/0012-821X(77)90060-7

Thirlwall, M. F., & Anczkiewicz, R. (2004). Multidynamic isotope ratio analysis using MC–ICP–MS and the causes of secular drift in Hf, Nd and Pb isotope ratios. *International Journal of Mass Spectrometry*, *235*(1), 59–81. https://doi.org/10.1016/j.ijms.2004.04.002

Wiedenbeck, M., Alle, P., Corfu, F., Griffin, W. L., Meier, M., Oberli, F., et al. (1995). Three natural zircon standards for U-Th-Pb, Lu-Hf, trace element and REE analyses. *Geostandards and Geoanalytical Research*, *19*, 1–23. https://doi.org/10.1111/j.1751-908X.1995.tb00147.x

Wiedenbeck, M., Hanchar, J. M., Peck, W. H., Sylvester, P., Valley, J., Whitehouse, M., et al. (2004). Further Characterisation of the 91500 zircon crystal. *Geostandards and Geoanalytical Research*, *28*(1), 9–39. https://doi.org/10.1111/j.1751908X.2004.tb01041.x

Williams, I. S. (1998). U–Th–Pb geochronology by ion microprobe. In M. A. McKibben, W. C. ShanksIII, & W. I. Ridley (Eds.), *Applications of microanalytical techniques to understanding mineralizing processes* (pp. 1–35). Society of Economic Geologists.